iScience

CellPress

Article

Tonotopic Differentiation of Coupling between Ca^{2+} and Kv1.1 Expression in Brainstem Auditory Circuit

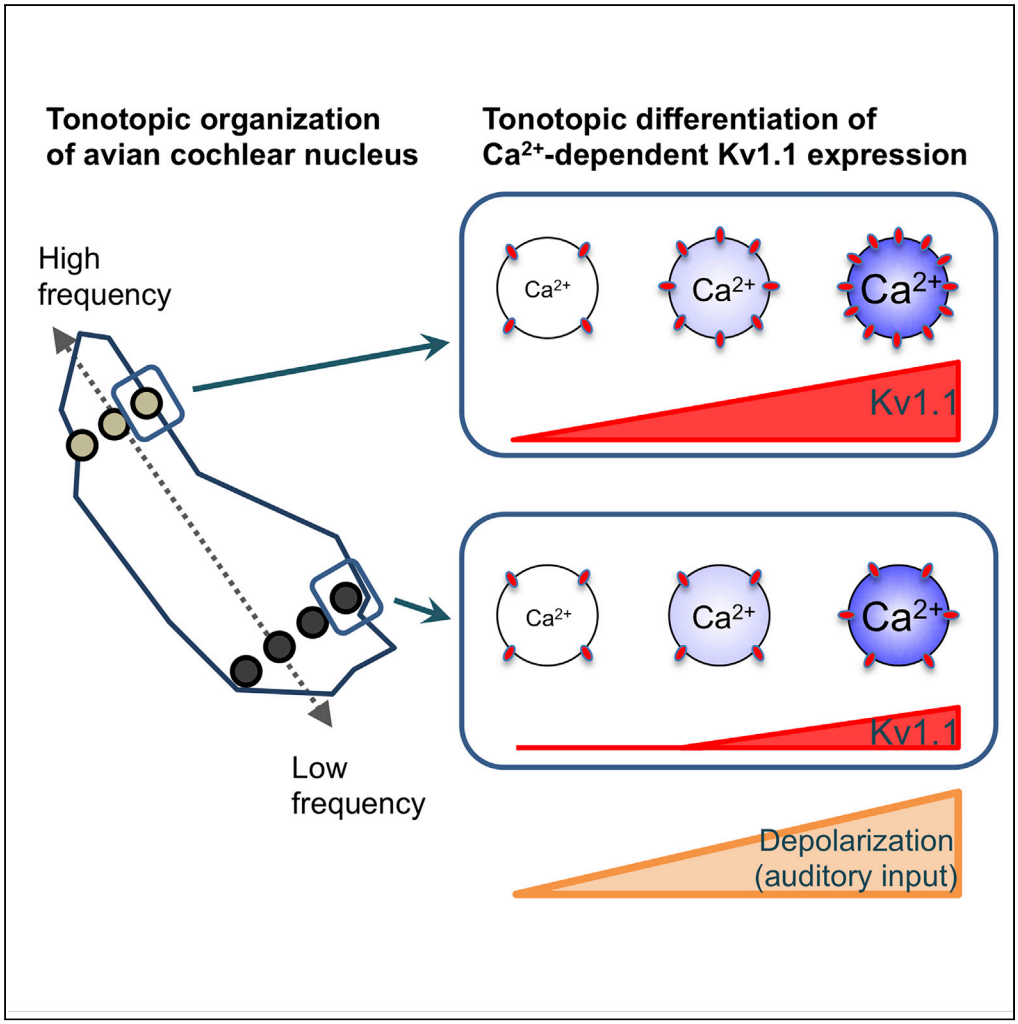

Ryota Adachi, Rei Yamada, Hiroshi Kuba

kuba@med.nagoya-u.ac.jp

HIGHLIGHTS

Kv1.1 expression is down-regulated in slice culture of chicken cochlear nucleus

Depolarization up-regulates Kv1.1 in a tonotopic-region-specific manner

Level of Kv1.1 expression is dependent on basal calcium concentration

Efficiency of calcium-dependent Kv1.1 expression is differentiated tonotopically

Adachi et al., iScience *13*, 199–213
March 29, 2019
https://doi.org/10.1016/j.isci.2019.02.022

iScience

CellPress

Article

Tonotopic Differentiation of Coupling between Ca^{2+} and Kv1.1 Expression in Brainstem Auditory Circuit

Ryota Adachi,[1] Rei Yamada,[1] and Hiroshi Kuba[1,2,*]

SUMMARY

Tonotopic differentiations of ion channels ensure sound processing across frequencies. Afferent input plays a critical role in differentiations. We demonstrate here in organotypic culture of chicken cochlear nucleus that expression of Kv1.1 was coupled with Ca^{2+} to a different degree depending on tonotopic regions, thereby differentiating the level of expression within the nucleus. In the culture, Kv1.1 was down-regulated and not differentiated tonotopically. Chronic depolarization increased Kv1.1 expression in a level-dependent manner. Moreover, the dependence was steeper at higher-frequency regions, which restored the differentiation. The depolarization increased Kv1.1 via activation of Cav1 channels, whereas basal Ca^{2+} level elevated similarly irrespective of tonotopic regions. Thus, the efficiency of Ca^{2+}-dependent Kv1.1 expression would be fine-tuned in a tonotopic-region-specific manner, emphasizing the importance of neuronal tonotopic identity as well as pattern of afferent input in the tonotopic differentiation of the channel in the auditory circuit.

INTRODUCTION

Precise temporal coding of sound requires proper adjustment of ion channel expression in auditory neurons (Johnston et al., 2010). Two types of voltage-gated K^+ (Kv) channels, Kv1.1 and Kv3.1, play central roles in the temporal coding. These channels mediate low- and high-voltage-activated K^+ currents, respectively. Kv1.1 is activated strongly at subthreshold potential and improves phasic firing by suppressing aberrant spike generation during synaptic depolarization, whereas Kv3.1 accelerates falling phase of spikes and promotes firing at high frequency (Oertel, 1999; Trussell, 1999).

Avian nucleus magnocellularis (NM), a homolog of mammalian anteroventral cochlear nucleus, is involved in the temporal coding (Sullivan and Konishi, 1984; Warchol and Dallos, 1990) and well known for rich expression of these Kv channels (Fukui and Ohmori, 2004; Parameshwaran et al., 2001; Rathouz and Trussell, 1998; Reyes et al., 1994). NM neurons are tuned to a specific frequency of sound (characteristic frequency, CF), and arranged tonotopically within the nucleus such that neurons with high CF are located rostromedially (Parks and Rubel, 1978). Moreover, they are differentiated biophysically as well as morphologically along the tonotopic axis (Fukui and Ohmori, 2004; Kuba and Ohmori, 2009; Oline et al., 2016; Wang et al., 2017). One prominent example is the differentiation of Kv1.1; the expression level of this channel increases in neurons with higher CF, which is considered crucial in adjusting neuronal excitability to the CF-specific patterns of afferent input in NM (Fukui and Ohmori, 2004). Recently, we reported that the differentiation of Kv1.1 was created because afferent input augmented the expression to a larger extent in higher-CF neurons (Akter et al., 2018), showing the importance of afferent input in setting the level of Kv1.1 expression. Intriguingly, however, the auditory threshold is higher for higher-frequency sound (Jones et al., 2006; Saunders et al., 1973), and therefore, the level of afferent input cannot solely explain the graded expression of Kv1.1 toward higher CF, raising a possibility that additional factors may contribute to the differentiation.

Thus, we explored the mechanisms of tonotopic differentiation of Kv1.1 in NM, using organotypic culture of chicken brainstem (Sanchez et al., 2011), in which neurons were totally deprived of afferent input. We found that chronic depolarization increased Kv1 current in a level-dependent manner, but the extent was larger at higher-CF regions, causing the tonotopic difference of the current in the culture. The depolarization increased Kv1 current via elevation of $[Ca^{2+}]_i$, whereas it elevated $[Ca^{2+}]_i$ similarly irrespective of tonotopic regions. The results showed that the Ca^{2+}-dependent process of Kv1.1 expression was more efficient at

[1]Department of Cell Physiology, Graduate School of Medicine, Nagoya University, Nagoya 466-8550, Japan

[2]Lead Contact

*Correspondence: kuba@med.nagoya-u.ac.jp

https://doi.org/10.1016/j.isci.2019.02.022

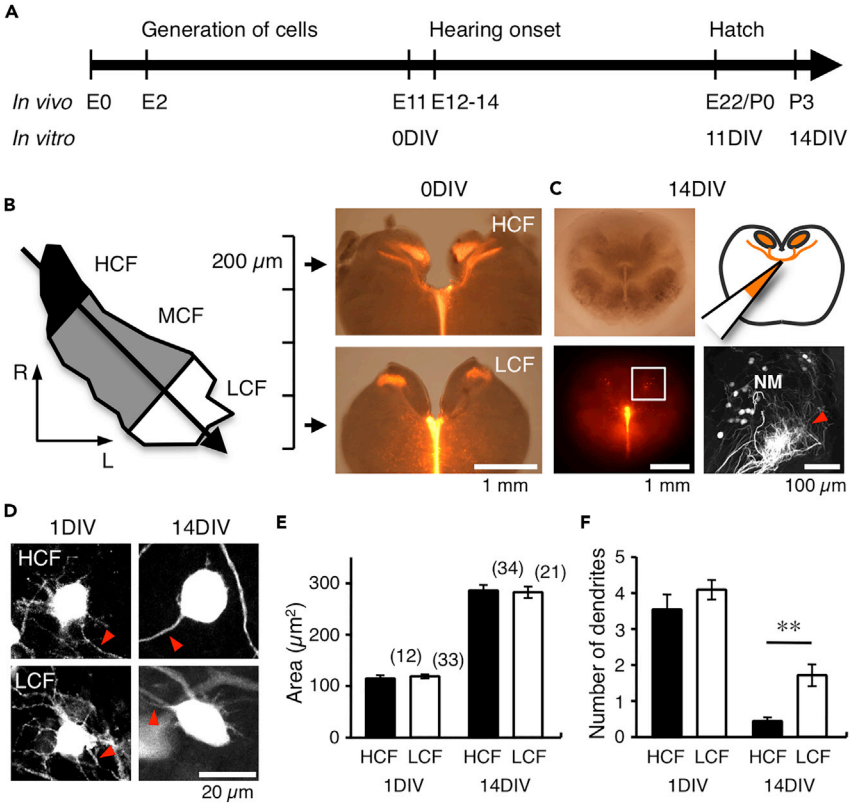

Figure 1. High- and Low-CF NM Neurons in Slice Culture

(A) Development of chicken auditory system *in vivo* and *in vitro*.

(B) NM is organized tonotopically from rostromedial to caudolateral direction. Four to five slices of 200 μm thickness were prepared from an animal at E11 after retrograde labeling of NM neurons with dextran TMR. NM in rostral one or two slices was defined as high-CF (HCF) region and that in the caudal most slice as low-CF (LCF) region.

(C) Cultured slice at 14DIV. NM was labeled with dextran TMR (upper right). Bright-field (upper left) and fluorescence (lower left) images of the slice. Square was magnified (lower right). Anterogradely labeled projections from contralateral NM (arrowhead).

(D) Retrogradely labeled NM neurons in high- (upper) and low-CF regions (lower) at 1DIV (left) and 14DIV (right). Arrowheads indicate axon.

(E and F) Cross-sectional area (E) and the number of dendrites (F) of cultured neurons. Numbers in parentheses are the number of cells. **$p < 0.01$.

See also Figure S1.

higher-CF regions, suggesting the importance of neuronal tonotopic identity as well as pattern of afferent input for the tonotopic differentiation of Kv1.1 in NM.

RESULTS

Characteristics of NM Neurons in Slice Culture

Brainstem slices were prepared from chicken embryos (embryonic day 11, E11) before hearing onset, and those including high- or low-CF neurons were cultured and used for experiments at 14 days *in vitro* (14DIV), corresponding to posthatch day 3 (P3) (Figures 1A and 1B). An injection of dextran tetramethylrhodamine (TMR) into the midline tract region visualized NM neurons and projection fibers from contralateral NM (Figure 1C). The morphology of NM neurons developed during the course of culture; the neurons showed multipolar shape and several dendrites at 1DIV but became spherical shape and decreased the number of dendrites by 14DIV (Figure 1D). Importantly, the loss of dendrites was more prominent in higher-CF neurons, making the neurons almost adendritic at 14DIV (Figure 1F), which resembled the morphological development *in vivo* (Jhaveri and Morest, 1982). Cross-sectional area of the soma increased with development and became similar between high- and low-CF neurons (Figure 1E).

	Control		High K^+ (1.5K)	
	High CF (n = 18)	Low CF (n = 17)	High CF (n = 7)	Low CF (n = 10)
Membrane property				
Rm (MΩ)	62.2 ± 4.5	61.8 ± 4.7	19.0 ± 1.6[a,b]	35.0 ± 2.9[a]
Vm (mV)	−59.2 ± 1.3	−58.5 ± 1.0	−65.9 ± 2.2[b,c]	−56.0 ± 1.0
Cm (pF)	40.3 ± 1.8	45.6 ± 2.2	43.9 ± 3.9	48.6 ± 3.9
τm (ms)	2.4 ± 0.1	2.8 ± 0.2	0.8 ± 0.1[a,b]	1.7 ± 0.2[a]
No. of spike (1-nA input)	2.0 ± 0.2[d]	3.2 ± 0.5	1.0 ± 0.1[a,b]	1.6 ± 0.4
Action potential				
Th. current (nA)	0.3 ± 0.1	0.2 ± 0.1	1.5 ± 0.2[a,b]	0.3 ± 0.1
Th. potential (mV)	−42.3 ± 1.4	−45.3 ± 0.9	−44.7 ± 3.2	−41.7 ± 1.3[c]
Amplitude (mV)	44.3 ± 1.4	47.2 ± 2.3	22.8 ± 1.9[a,b]	49.2 ± 1.5
Half-width (ms)	0.5 ± 0.1[d]	0.4 ± 0.1	0.3 ± 0.1[a,b]	0.5 ± 0.1
Max. dV/dt (V/s)	224.2 ± 12.9	255.5 ± 16.8	148.5 ± 9.1[a,b]	242.9 ± 13.7
Mini. dV/dt (V/s)	−105.5 ± 7.6[d]	−127.8 ± 7.6	−127.9 ± 6.8	−129.2 ± 7.9
Latency (ms)	2.3 ± 0.1	2.3 ± 0.1	1.1 ± 0.1[a,b]	2.1 ± 0.1

Table 1. Parameters of Membrane Property and Action Potential

Input resistance (Rm), resting potential (Vm), membrane capacitance (Cm), and membrane time constant (τm).

[a]$p < 0.01$ (between control and high-K^+ condition).

[b]$p < 0.01$ (between high- and low-CF neurons).

[c]$p < 0.05$ (between control and high-K^+ condition).

[d]$p < 0.05$ (between high- and low-CF neurons).

We also evaluated excitatory synaptic input in the cultured NM neurons at 11DIV (Figure S1A). Auditory nerve terminals are differentiated tonotopically in NM *in vivo*; they form end-bulb synapses on high-CF neurons and bouton synapses on low-CF neurons (Fukui and Ohmori, 2004; Köppl, 1994). Although the auditory nerve was lost in the culture, multiple VGlut2-positive glutamatergic terminals apposed on both high- and low-CF neurons (Figures S1B and S1E). The number and size of these terminals were similar between the neurons. Consistently, both neurons showed spontaneous excitatory postsynaptic currents (EPSCs) of similar amplitude and rate in the culture medium (Figures S1C, S1F, and S1H–S1J). However, the amplitude of EPSCs was mostly below 100 pA, the rate was low (6–7 Hz), and their contributions to spike generation would be small. Indeed, when spontaneous spikes were recorded under cell-attached clamp, the rate (<1 Hz) was far lower than that of spontaneous EPSPs (1–2 Hz) (Figures S1D, S1G, S1K, and S1L) and almost negligible compared with that *in vivo* (100–500 Hz, Fukui et al., 2006; Warchol and Dallos, 1990). Thus, the culture was preferable in evaluating the mechanism of tonotopic differentiation of Kv1.1 expression in NM under the minimal influence of synaptic and spike activities.

Membrane Properties Were Similar in Cultured High- and Low-CF Neurons

Membrane parameters of cultured NM neurons were measured at 14DIV, corresponding to P3, by injecting a rectangular current to the soma under current clamp (Table 1). The input resistance was larger and the resting potential was more positive than those in posthatch neurons in acute slices (see Akter et al., 2018), suggesting a decrease of Kv1 current in the culture. More importantly, the parameters were not different between high- and low-CF neurons. This contrasted with the clear tonotopic differences in the parameters in acute slices, such as lower input resistance and more negative resting potential in higher-CF neurons (Akter et al., 2018; Fukui and Ohmori, 2004), indicating that the tonotopic differentiation of Kv1 current would be small or absent in the culture.

We then examined voltage responses to currents between −0.5 and 2 nA in the culture (Figure 2). Both high- and low-CF neurons showed outward-rectifying responses and generated one or a few spikes at

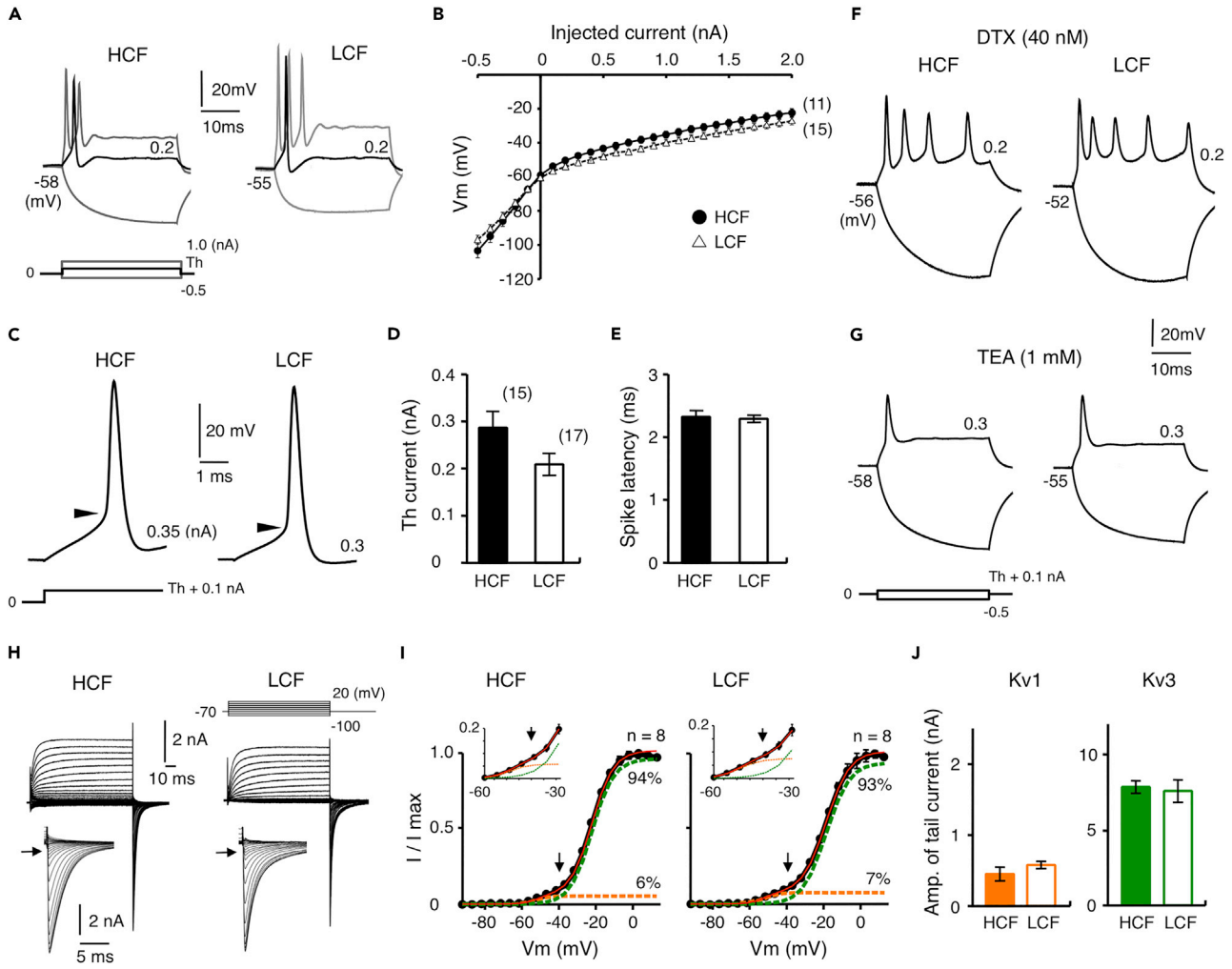

Figure 2. Kv1 Current Was Not Differentiated Tonotopically in Culture

(A) Voltage responses to current injection (30 ms) between −0.5 and 2 nA with a 0.1-nA step at 14DIV. High- (left) and low-CF (right) neurons. Traces at −0.5 and 1 nA (gray) and that at threshold current (black) are shown. Membrane potential is indicated at left.

(B) Voltage-current relationship measured at pulse end.

(C) Action potentials at 0.1 nA above threshold current. Arrowheads indicate threshold potential.

(D and E) Threshold current (D) and latency (E) of spikes. Numbers in parentheses are the number of cells.

(F and G) Voltage responses in the presence of 40 nM DTX (F) or 1 mM TEA (G). Traces at −0.5 nA and 0.1 nA above threshold current are shown.

(H) Kv current recorded with voltage pulses (100 ms) between −100 and +20 mV at −70 mV. Tail current was expanded (inset). High- (left) and low-CF (right) neurons.

(I) Conductance-voltage curve of tail current. Magnified curve (inset). The curve was fitted to a double Boltzmann equation (red), and Kv1 and Kv3 components were shown in orange and green, respectively. Arrows indicate tail current at −40 mV and roughly represents Kv1 current.

(J) Kv1 (left, orange) and Kv3 (right, green) currents calculated at +20 mV.

See also Figure S2.

the onset of depolarization (Figures 2A and 2B), as in acute slices (Akter et al., 2018; Fukui and Ohmori, 2004). Bath application of dendrotoxin (DTX, 40 nM, blocker of Kv1) increased the number of spikes; the number was 3.3 ± 0.4 (n = 10) ($p = 3.9\times10^{-6}$; compared with control, 0.9 ± 0.1, n = 15) and 3.9 ± 0.4 (n = 8) ($p = 3.7\times10^{-6}$; compared with control, 1.2 ± 0.2, n = 17) in high- and low-CF neurons, respectively (p = 0.29) (Figure 2F). On the other hand, tetraethylammonium (TEA, 1 mM, blocker of Kv3) increased the half-width of spikes; the increase was 158% (n = 6) ($p = 8.2\times10^{-6}$) and 211% (n = 4) ($p = 2.9\times10^{-10}$) in high- and low-CF neurons, respectively (p = 0.08) (Figure 2G), confirming the presence of Kv1 and Kv3 currents in the neurons. The level of outward rectification was similar between the high- and low-CF neurons (Figure 2B). Moreover, many spike parameters, including threshold current and spike latency, did not differ

	Control		High K^+ (1.5K)	
	High CF (n = 8)	Low CF (n = 8)	High CF (n = 10)	Low CF (n = 8)
Kv1 current (nA)	0.5 ± 0.1	0.6 ± 0.1	2.1 ± 0.2[a,b]	0.9 ± 0.1[a]
Kv3 current (nA)	7.7 ± 0.4	7.6 ± 0.7	9.7 ± 0.6[c]	10.1 ± 1.0[c]
Kv1 $V_{1/2}$ (mV)	−51.4 ± 0.8	−51.8 ± 0.7	−53.4 ± 0.6[c]	−53.1 ± 1.0
Kv3 $V_{1/2}$ (mV)	−21.6 ± 0.5	−19.4 ± 1.1	−20.0 ± 0.7	−18.5 ± 1.3
Kv1 slope (mV)	3.5 ± 0.3	4.0 ± 0.2	4.7 ± 0.2[a]	4.7 ± 0.8
Kv3 slope (mV)	5.8 ± 0.2	5.9 ± 0.1	5.7 ± 0.1	6.3 ± 0.2

Table 2. Parameters of Kv Current

[a]$p < 0.01$ (between control and high-K^+ condition).

[b]$p < 0.01$ (between high- and low-CF neurons).

[c]$p < 0.05$ (between control and high-K^+ condition).

between the neurons (Table 1; Figures 2C–2E), being compatible with the idea that the tonotopic differentiation of Kv1 current was almost absent in the culture. Nevertheless, a 1-nA current generated more spikes and their falling phase was accelerated in low-CF neurons (Table 1), and therefore, small differences of Kv currents could be present between the neurons.

Kv Current Was Similar in Cultured High- and Low-CF Neurons

We compared Kv current between high- and low-CF neurons at 14DIV under voltage clamp, using a Cs^+-based internal solution with voltage pulses (100 ms) between −100 and +20 mV at a holding potential of −70 mV (Figure 2H). An outward current appeared during the test pulse, and an inward tail current (inset) followed after cessation of the pulse in both neurons. The current would be mediated via Kv1 and Kv3 currents (see Kuba et al., 2015; Rathouz and Trussell, 1998). Voltage-dependence of activation of Kv current was evaluated via plotting conductance-voltage curve of the tail current and fitting it to a double Boltzmann equation (Figure 2I; Table 2). Kv1 current was identified as the low-voltage-activated component with a $V_{1/2}$ of about −50 mV and Kv3 current as the high-voltage-activated component with a $V_{1/2}$ of about −20 mV in both neurons. Remarkably, Kv1 current was small and similar in both neurons (0.4–0.6 nA, 6%–7% of total current) (Figures 2I and 2J), which was 3–10 times smaller than that in posthatch neurons (Akter et al., 2018). The results indicated that the expression of Kv1.1 was down-regulated in the culture and not differentiated tonotopically, being consistent with the findings in current clamp experiments (see Figures 2A–2E). On the other hand, Kv3 current was two times larger than that in posthatch neurons (7–8 nA, 93%–95% of total current) (Figures 2I and 2J; see Akter et al., 2018).

Kv current increased during the course of culture from 5.0 ± 0.3 nA (n = 15) at 4DIV to 8.1 ± 0.4 nA (n = 8) at 14DIV, whereas Kv1 current did not change during the period; it was 0.3 ± 0.1 nA (7% of total current, n = 15) and 0.5 ± 0.1 nA (6% of total current, n = 8) for 4DIV and 14DIV, respectively ($p = 0.4$). This tendency was similar in neurons cultured with tetrodotoxin (TTX) (0.1 μM) (three cells), suggesting that spontaneous activities had little effects on Kv1 current in the culture. The results also indicated that Kv3 current could increase without postsynaptic depolarization, which agreed with the observations in otocysts-removed animals (Akter et al., 2018).

Chronic Depolarization Increased Kv1 Current More Efficiently in High-CF Neurons

Auditory input is important for the expression of Kv1.1 in NM neurons (Akter et al., 2018). Thus, we mimicked the effect of auditory input in the culture, through chronic depolarization via elevating $[K^+]_o$ in the culture medium by 1.5 times (7.95 mM, 1.5K medium) for 13 days between 1DIV and 14DIV (Figure 3A). After the treatment with 1.5K medium, the resting potential became more negative (5 mV) in normal artificial cerebrospinal fluid (ACSF) and the input resistance decreased by three times in high-CF neurons (Table 1). In addition, the treatment augmented the outward rectification, shortened the spike latency by half, and increased the threshold current by five times in the neurons (Figures 3B–3D; Table 1), suggesting that the chronic depolarization increased Kv1 current in the high-CF neurons. Accordingly, the number of spikes decreased and spikes were no longer generated at 1 nA (Figure 3B). In low-CF neurons, on the other hand,

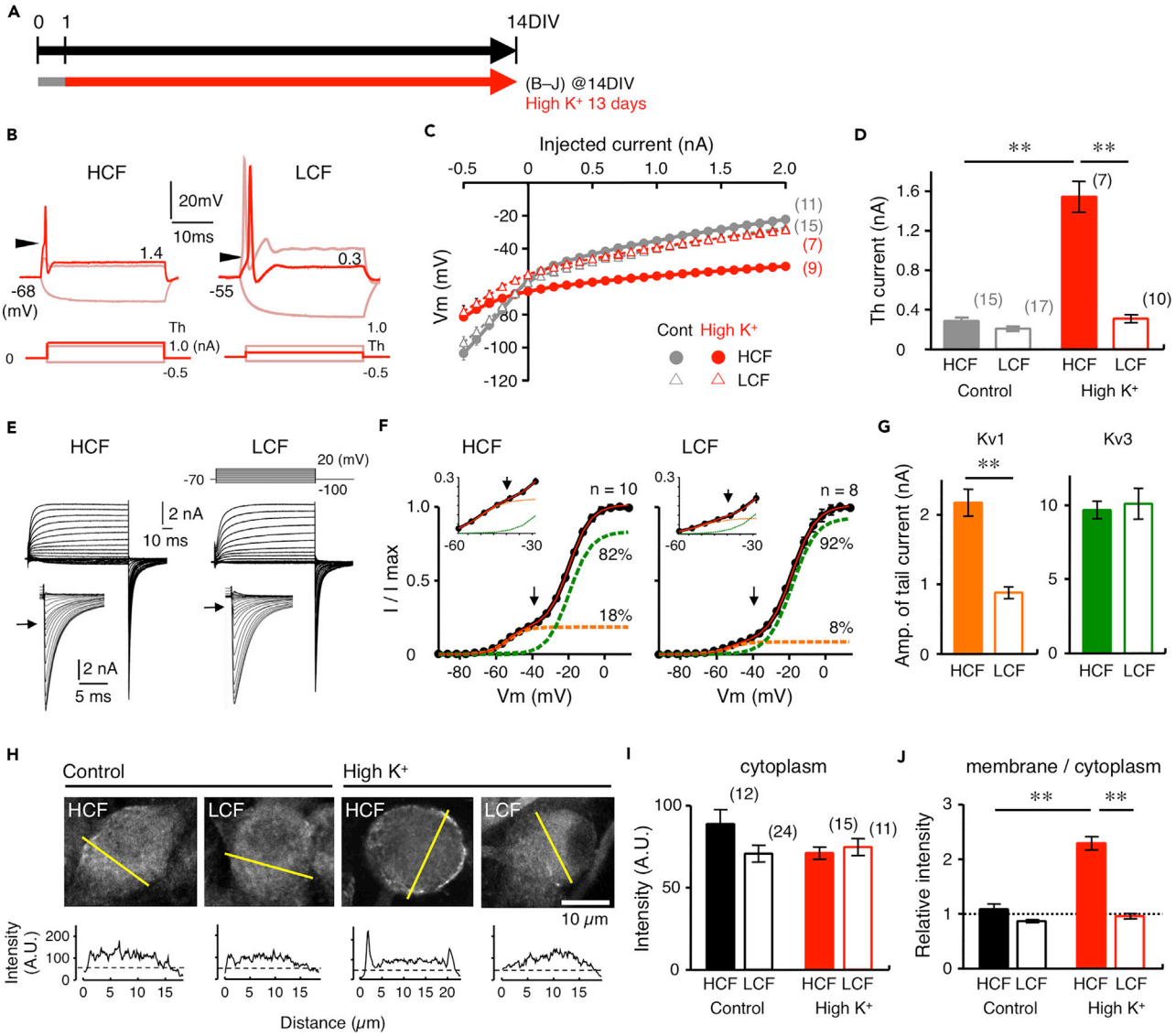

Figure 3. Chronic Depolarization Restored Tonotopic Differentiation of Kv1 Current

(A) $[K^+]_o$ in culture medium was elevated by 1.5 times (7.95 mM) for 1–14DIV by adding KCl to culture medium.

(B) Voltage responses to current injection after chronic depolarization. High- (left) and low-CF (right) neurons. Traces at −0.5 and 1 nA (thin) and that at threshold current (thick) are shown. Arrowheads indicate threshold potential.

(C) Voltage-current relationship measured at pulse end. Controls were from Figure 2B (gray).

(D) Threshold current of spikes. Controls were from Figure 2D (gray). Numbers in parentheses are the number of cells.

(E) Kv current after chronic depolarization. Tail current was expanded (inset). High- (left) and low-CF (right) neurons.

(F) Conductance-voltage curve of tail current. Magnified curve (inset). The curve was fitted to a double Boltzmann equation (red), and Kv1 and Kv3 components were shown in orange and green, respectively. Arrows indicate tail current at −40 mV, and roughly represents Kv1 current.

(G) Kv1 (left, orange) and Kv3 (right, green) currents calculated at +20 mV. Note that Kv1 current became larger by 4.5 times in high-CF neurons and 1.5 times in low-CF neurons after chronic depolarization.

(H) Immunostaining of Kv1.1 at 14DIV in control and after chronic depolarization (upper). High- (left) and low-CF (right) neurons. Intensity profile was plotted along a line (yellow) across the cells (lower).

(I and J) Signal intensity at cytoplasmic region (I) and relative intensity between membranous and cytoplasmic regions (J). Note that membranous signal was augmented in high-CF neurons after the depolarization.

**$p < 0.01$.

input resistance decreased, but spike latency and threshold current did not change after the treatment, and most neurons still generated more than one spike at 1 nA.

The inward tail current increased in both neurons after the treatment with 1.5K medium (Figure 3E). However, the increase of Kv1 current was far larger in high-CF neurons than in low-CF neurons, creating a tonotopic difference of Kv1 current in the culture; the increase was about 5 times (2.1 ± 0.2 nA, 18% of total current) and 1.3 times (0.9 ± 0.1 nA, 8% of total current) in high- and low-CF neurons, respectively (Figures 3F and 3G; Table 2). In addition, strong immunosignals of Kv1.1 delineated the cell soma after the treatment specifically in the high-CF neurons with little changes in cytoplasmic signals (Figures 3H–3J). Importantly, the differential increase of Kv1 current occurred even when slices from different tonotopic regions were cultured on the same Millicell membrane (data not shown), suggesting that contributions of diffusible factors to the differentiation could be small. These results indicated that efficiency to drive Kv1.1 expression via depolarization would differ tonotopically in NM, being higher in high-CF neurons, which was consistent with the observations *in vivo* (Akter et al., 2018). Kv3 current increased slightly after the treatment, but the increase was about 1.3 times and did not differ between high- and low-CF neurons (Figure 3G; Table 2).

Increase of Kv1 Current Was Dependent on Level of Depolarization

We then examined the effects of the level of depolarization on the increase of Kv1 current (Figure 4A). Membrane was depolarized for 3 days between 11DIV and 14DIV, corresponding to P0–3, at which activity-dependent increase of Kv1 current occurs *in vivo*, via elevating $[K^+]_o$ in the culture medium by 1.5 times (7.95 mM, 1.5K medium), 2 times (10.6 mM, 2K medium), or 3 times (15.9 mM, 3K medium). The level of depolarization increased upon high-K^+ treatment in a manner dependent on $[K^+]_o$ irrespective of tonotopic regions, and the membrane remained depolarized at 14DIV, although the depolarization decreased slightly during the high-K^+ treatment particularly in high-CF neurons, likely reflecting the increase of Kv1.1 expression in the neurons (Table 3). In the high-CF neurons, the treatment with 1.5K medium increased Kv1 current by five times (2.1 ± 0.5 nA, 22% of total current) (Figures 4B and 4G), and the extent was similar to that after 13 days of treatment (1–14DIV) (see Figures 3E–3G), indicating that 3 days of depolarization was sufficient for the increase of Kv1 current, as *in vivo* (Akter et al., 2018). Kv1 current increased further and reached a plateau after the treatment with 2K medium (3.9 ± 0.2 nA, 37% of total current) or 3K medium (3.9 ± 0.4 nA, 40% of total current) (Figures 4C, 4D, and 4G), and the size was comparable with that in posthatch neurons (4.2 nA, 53% of total current; Akter et al., 2018). In low-CF neurons, on the other hand, Kv1 current increased slightly with 3K medium (0.7 ± 0.1 nA, 9% of total current) but with neither 1.5K (0.4 ± 0.1 nA, 5% of total current) nor 2K (0.3 ± 0.1 nA, 5% of total current) medium (Figures 4E–4G). Thus, the level of Kv1.1 expression depended on the level of depolarization in NM neurons, but the dependence was much steeper in the high-CF neurons than in the low-CF neurons.

Importantly, Kv1 current increased in high-CF neurons even when $[K^+]_o$ was elevated between 7DIV and 10DIV, corresponding to E18–20 (Figures 4H–4J); the amplitude was 1.8 ± 0.2 and 2.6 ± 0.3 nA (22% and 35% of total current) for 1.5K and 2K media, respectively, suggesting that the mechanism of depolarization-dependent Kv1.1 expression might be already equipped in the neurons at embryonic periods.

We also evaluated the effects of the high-K^+ media on spontaneous activities in the culture (Figure S2A). When the cultures were bathed in the 1.5K medium at 11DIV, the rate of spontaneous EPSCs increased slightly but it was still low in both high- and low-CF neurons (about 10 Hz) (Figures S2B, S2D, and S2G). In addition, their amplitude decreased substantially in the medium (30–60 pA) (Figures S2B, S2D, and S2F). This occurred because large EPSCs were suppressed in the medium (see Figure S1H), presumably due to progressions of both Na^+ current inactivation and K^+ current activation in the presynaptic neurons. Consistently, spontaneous EPSPs and spikes were almost absent in the 1.5K medium in both neurons (<0.1 Hz) (Figures S2C, S2E, S2H, and S2I). Moreover, chronic treatment with 1.5K medium increased Kv1 current in the presence of TTX (0.1 μM), 6,7-dinitroquinoxaline-2,3-dione (DNQX) (20 μM), and D-AP5 (100 μM) in high-CF neurons (1.5 ± 0.2 nA, 19% of total current) (Figures S2J–S2L). These results indicated that the increase of Kv1 current would be primarily driven by chronic depolarization of NM neurons during the high-K^+ treatment in the culture.

Intracellular Cl^- level is high and E_{Cl} is depolarized in NM neurons (Hyson et al., 1995; Monsivais et al., 2000; Lu and Trussell, 2001). In addition, Cl^- permeability may increase when $[K^+]_o$ is elevated, affecting the level of

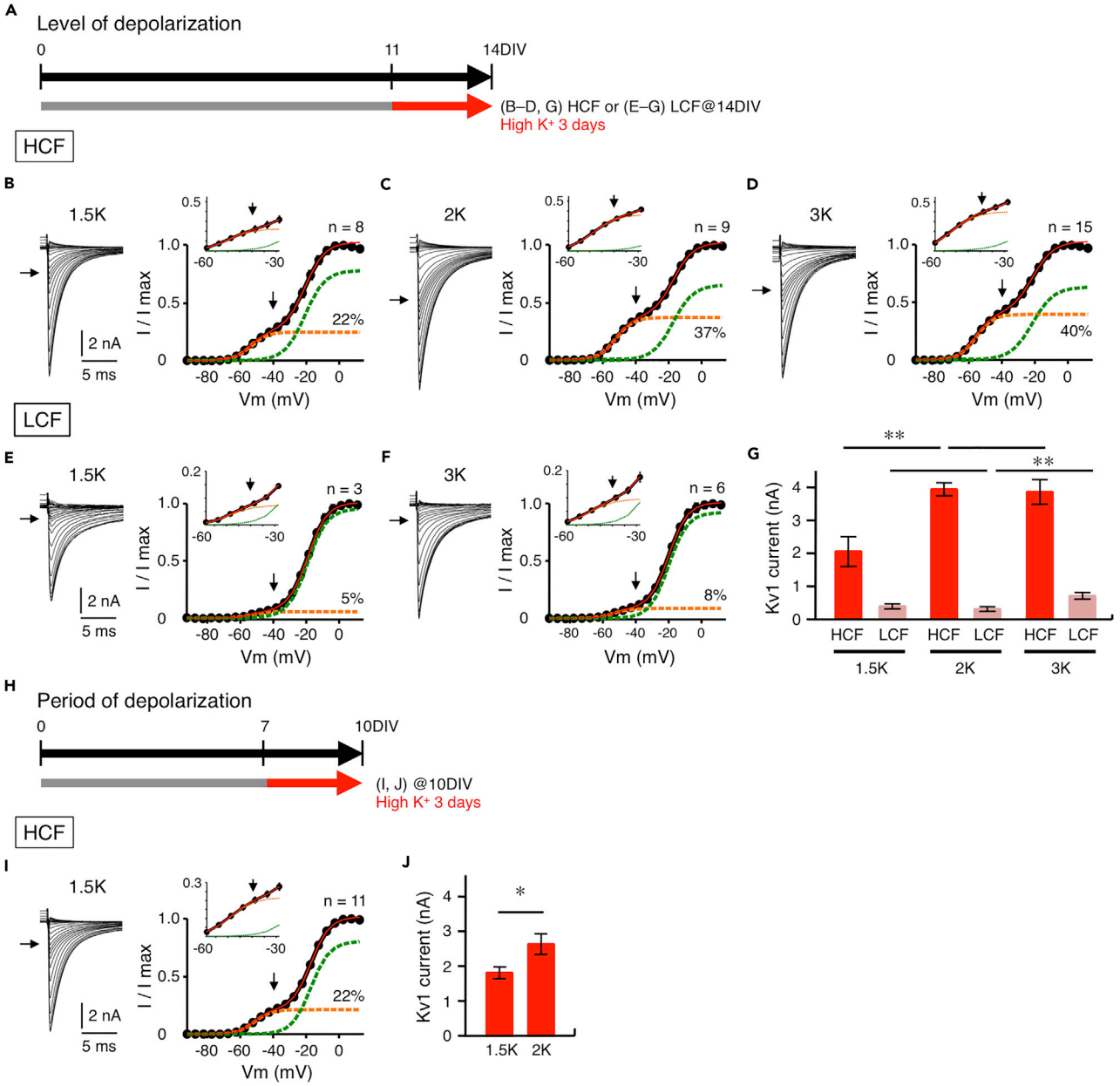

Figure 4. Increase of Kv1 Current Depended on Level of Depolarization but the Dependence Was Steeper in High-CF Neurons

(A) $[K^+]_o$ in culture medium was elevated by 1.5–3 times for 11–14DIV in high- and low-CF neurons.

(B–D) Effects of level of depolarization on Kv current in high-CF neurons. Tail current (left) and conductance-voltage curve (right) at 1.5 times (7.95 mM, B), 2 times (10.6 mM, C), and 3 times (15.9 mM, D) of $[K^+]_o$. The curve was fitted to a double Boltzmann equation (red), and Kv1 and Kv3 components were shown in orange and green, respectively. Arrows indicate tail current at −40 mV and roughly represents Kv1 current. Magnified curve (inset).

(E and F) Effects of level of depolarization on Kv current in low-CF neurons. Tail current (left) and conductance-voltage curve (right) at 1.5 times (E) and 3 times (F) of $[K^+]_o$. $[K^+]_o$ was not increased further, because the neurons could not survive in the medium.

(G) Kv1 current calculated at +20 mV at high- and low-CF regions. Note that Kv1 current increased more steeply with an elevation of $[K^+]_o$ in high-CF neurons.

(H–J) Effects of period of depolarization on Kv current in high-CF neurons. $[K^+]_o$ in culture medium was elevated for 7–10DIV, and recording was made at 10DIV (H). Tail current (left) and conductance-voltage curve (right) at 1.5 times of $[K^+]_o$ (I). Kv1 current calculated at +20 mV (J).

*p < 0.05, **p < 0.01. See also Figures S2 and S3.

depolarization via alterations of $[Cl^-]_i$ (Babot et al., 2005). However, this possibility would be low, because 1.5K medium did not change intracellular Cl^- level, when measured with a Cl^- dye (MQAE, see Transparent Methods), and the effects were similar with or without a cocktail of Cl^- channel blockers (Figure S3).

	Control	1.5K	2K	3K
High CF				
Onset	−53.2 ± 0.4 (n = 6)	−46.1 ± 0.7 (n = 7)	−40.4 ± 1.2 (n = 6)	−36.1 ± 1.3 (n = 6)
End	−55.6 ± 0.7 (n = 6)[a]	−52.7 ± 0.3 (n = 6)[b]	−45.3 ± 1.5 (n = 6)[a]	−39.0 ± 0.9 (n = 7)
Low CF				
Onset	−52.4 ± 0.7 (n = 9)	−45.6 ± 0.6 (n = 10)	−40.8 ± 0.6 (n = 7)	−35.5 ± 0.8 (n = 5)
End	−56.0 ± 1.7 (n = 5)	−47.1 ± 1.1 (n = 9)[c]	−43.1 ± 1.0 (n = 9)	−37.4 ± 0.4 (n = 8)[a]

Table 3. Effects of High-K^+ Treatment on Membrane Potential

Membrane potential was measured at onset (11DIV) and end (14DIV) of 3-day treatment in the corresponding culture medium.

[K^+] was 5.3 mM, 7.95, 10.6, and 15.9 mM for control, 1.5K, 2K, and 3K medium, respectively.

High- K^+ treatment depolarized the membrane ($p < 0.01$, compared with control), and the level of depolarization depended on [K^+].

[a] $p < 0.05$ (between onset and end of high- K^+ treatment).

[b] $p < 0.01$ (between onset and end of high- K^+ treatment).

[c] $p < 0.01$ (between high- and low-CF neurons).

Elevation of $[Ca^{2+}]_i$ Increased Kv1 Current More Efficiently in High-CF Neurons

Depolarization is expected to elevate intracellular Ca^{2+} level via activation of Cav channels. Various types of Cav channels are reported in NM neurons, including L-type (Cav1), P/Q-type (Cav2.1), N-type (Cav2.2), R-type (Cav2.3), and T-type (Cav3) channels (Koyano et al., 1996; Lu and Rubel, 2005). We tested the contributions of these channels to the increase of Kv1 current by depolarizing the tissues with elevated $[K^+]_o$ (1.5K medium) and then by concurrently applying Cav channel blockers between 11DIV and 14DIV (Figure 5A). Nifedipine (10 μM, blocker of Cav1) or (+)-Bay-K8644 (5 μM, blocker of Cav1) occluded the increase of Kv1 current during the depolarization (0.7 ± 0.1 nA, 8% of total current for nifedipine; 0.7 ± 0.1 nA, 11% for (+)-Bay-K8644), whereas ω-conotoxin GVIA (2 μM, blocker of Cav2.2) did not affect the increase of the current (2.1 ± 0.4 nA, 19% of total current) (Figures 5B, 5C, and S4). Further application of ω-agatoxin IVA (0.2 μM, blocker of Cav2.1), $NiCl_2$ (100 μM, blocker of Cav2.3 and Cav3), and TTA-P2 (2 μM, blocker of Cav3) did not show additional effects (0.9 ± 0.1 nA, 8% of total current). In addition, nifedipine did not affect spontaneous EPSCs in the 1.5K medium; the rate was 11.5 ± 3.2 Hz ($n = 7$, $p = 0.84$ compared with 1.5K medium). These results indicated that elevation of Ca^{2+} level was necessary for the increase of Kv1 current and it was mediated via postsynaptic Cav1 channels in the culture.

We then examined Ca^{2+} level in high- and low-CF neurons with a two-photon microscope at 11DIV (Figure 5D). Cells were loaded with a high-affinity Ca^{2+} indicator (OGB-1, G) and a volume marker (Alexa 594, R) through a patch pipette, and line scans were made across the cells (red lines), while a depolarizing current was applied under voltage clamp (Figures 5E–5G). Upon depolarization, the Ca^{2+} signal (G/R) increased in both neurons. More importantly, the increase (ΔG/R) depended on the level of depolarization. Indeed, when $[Ca^{2+}]_i$ was measured at various holding potentials with a low-affinity Ca^{2+} indicator (Fluo-5F), a similar depolarization dependence of $[Ca^{2+}]_i$ was observed and it was blocked with nifedipine or (+)-Bay-K8644 (Figures 5H, 5I, and S4). Remarkably, $[Ca^{2+}]_i$ was rather low (below 200 nM) even at −40 mV, comparable with the membrane potential in the 2K medium. The results indicated that a slight change in the basal Ca^{2+} level would critically affect the expression of Kv1.1 and fine adjustment of the Ca^{2+} level should be the key in setting the level of Kv1.1 expression. To our surprise, however, the elevation of $[Ca^{2+}]_i$ did not differ between the high- and low-CF neurons (Figure 5G). In addition, Cav1 mRNAs were expressed similarly at both regions (Figure S5). These findings suggested that downstream mechanisms of Ca^{2+} would be differentiated between the high- and low-CF neurons, contributing to the tonotopic-region-specific increase of Kv1 current during the depolarization.

$[Ca^{2+}]_i$ in 1.5K medium was also measured at 14DIV after incubating slices for 3 days in the medium, and it was still dependent on depolarization and comparable with that measured at 11DIV in normal ACSF (Figure S6, see Figure 5I). Although it was not significant, the dependence tended to become weaker after the treatment, and this might reflect rundown or inactivation of Cav channels during the depolarization.

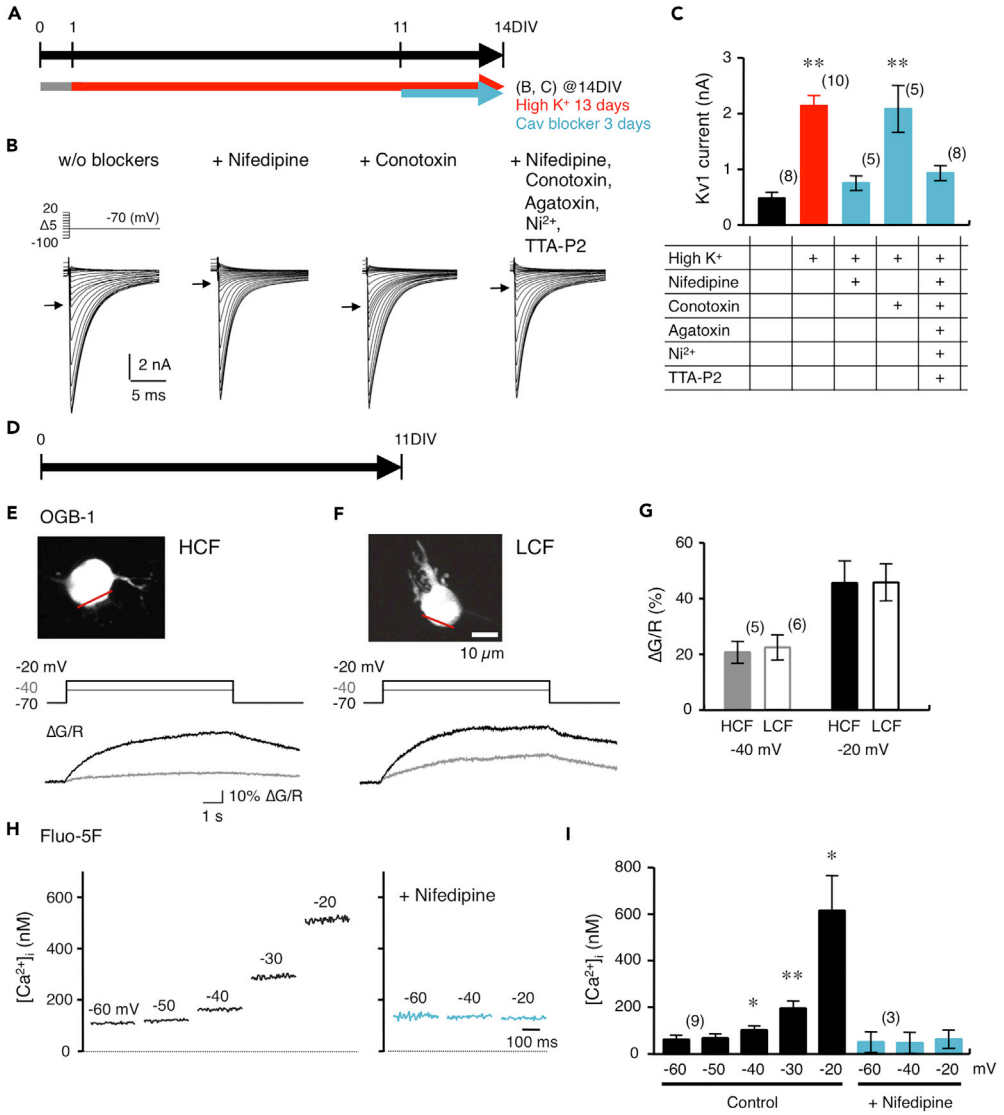

Figure 5. Chronic Depolarization Elevated Basal Ca^{2+} Level Similarly Irrespective of Tonotopic Regions

(A–C) Effects of Cav channel blockers on increase of Kv current during depolarization in high-CF neurons. $[K^+]_o$ in culture medium was elevated by 1.5 times, while Cav channel blockers were added for 11–14DIV (A). Tail current without blockers (left), after the treatment of nifedipine (10 μM, left middle), ω-conotoxin GVIA (2 μM, right middle), and cocktail of blockers (right) (B). Arrows indicate tail current at −40 mV, and roughly represents Kv1 current. Kv1 current calculated at +20 mV in high-CF neurons (C). Data in control (black) and 1.5K treatment (red) were from Figures 2J and 3G. Numbers in parentheses are the number of cells. **p < 0.01 compared with control.

(D) Neurons were cultured in normal medium, and two-photon imaging was made at 11DIV.

(E and F) Ca^{2+} signals in high- (E) and low-CF (F) neurons. Cells were loaded with a high-affinity indicator (OGB-1, G) and Alexa 594 (R) through a patch pipette, and line scans were made at the soma (top, red line). ΔG/R increased in both neurons (bottom), when a depolarizing voltage pulse (10 s) was applied under voltage clamp (middle).

(G) ΔG/R at corresponding voltage.

(H) $[Ca^{2+}]_i$ measured with a low-affinity indicator (Fluo-5F) under voltage clamp.

(I) Dependence of $[Ca^{2+}]_i$ on membrane depolarization. Values were similar between high- and low-CF neurons ($p > 0.1$), and data from both neurons were combined. *p < 0.05, **p < 0.01 compared with −60 mV. Note that $[Ca^{2+}]_i$ was still within nanomolar range (about 200 nM) even at membrane potential comparable with that in 2K medium (−40 mV). The increase of $[Ca^{2+}]_i$ was occluded by nifedipine (10 μM, light blue). Cocktail of blockers in (B) showed similar suppression of $[Ca^{2+}]_i$; $[Ca^{2+}]_i$ in the cocktail was 117.3 ± 22.4 nM at −60 mV, 133.9 ± 34.5 nM at −40 mV, and 213.0 ± 70.8 nM at −20 mV (n = 5) ($p > 0.1$ compared with that of nifedipine at each voltage).

See also Figures S4–S6.

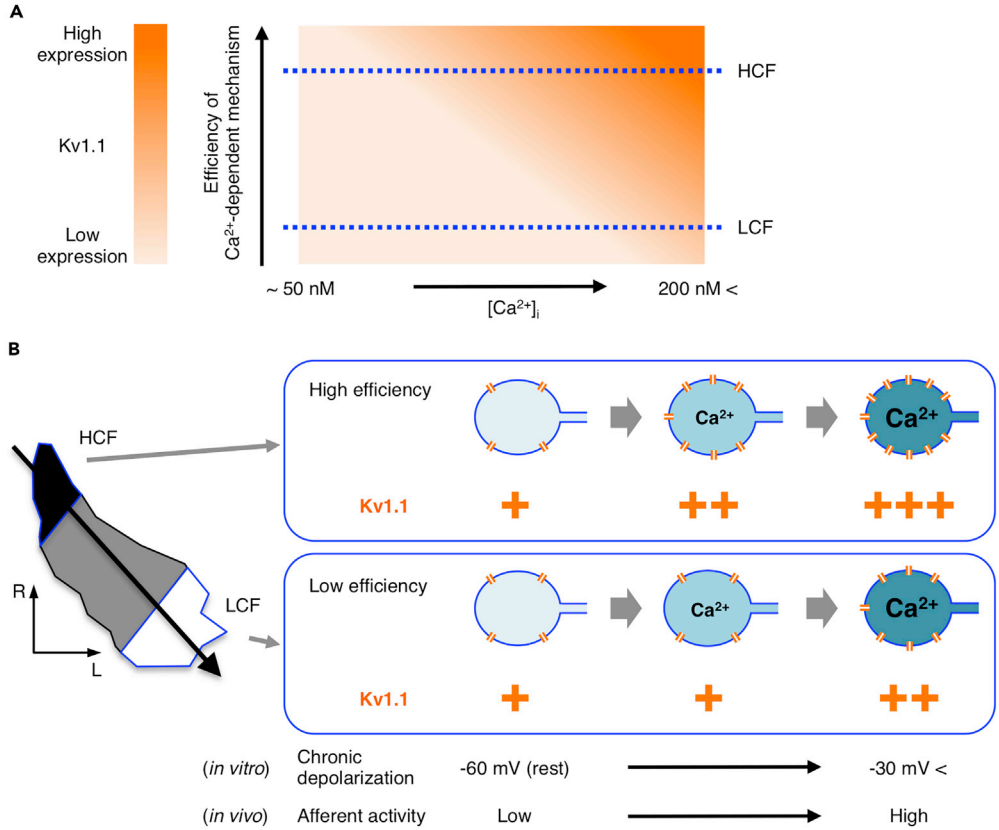

Figure 6. Efficiency of Translating Ca^{2+} Level into Kv1.1 Expression Would Be Differentiated along the Tonotopic Axis in NM

(A) Level of Kv1.1 expression is regulated via an interaction between "efficiency" of Ca^{2+}-dependent mechanism and $[Ca^{2+}]_i$. Note that Kv1.1 level is the same irrespective of efficiency at low $[Ca^{2+}]_i$, whereas the level increases more steeply at higher efficiency with an increase of $[Ca^{2+}]_i$. The efficiency would be higher in higher-CF neurons (dotted horizontal lines).

(B) Schematic drawing of relationship between $[Ca^{2+}]_i$ and Kv1.1 expression in high- and low-CF neurons. Kv1.1 increased with an increase of $[Ca^{2+}]_i$ in both neurons, but the dependence was steeper in high-CF neurons, causing higher expression of Kv1.1 in the neurons (orange). This implied that the coupling between Ca^{2+} and Kv1.1 expression would be determined in a tonotopic-region-specific manner, suggesting that genetic program as well as afferent activity would be crucial for the tonotopic-differentiation of Kv1.1 expression in NM. Note that the increase of $[Ca^{2+}]_i$ was mediated via activation of Cav1 channels during chronic depolarization in the culture, whereas the increase would be driven by afferent activity via activations of AMPA receptors and/or Cav channels *in vivo*.

DISCUSSION

Cultured NM neurons showed a tonotopic difference of Kv1 current only when the neurons were chronically depolarized with high-K^+ media. This occurred because the increase of Kv1 current was dependent on the level of depolarization, and the dependence was steeper in higher-CF neurons. Blockade of Cav1 channels suppressed the increase of Kv1 current and the differentiation. In addition, depolarization elevated $[Ca^{2+}]_i$ similarly irrespective of tonotopic regions. These findings suggested that the Ca^{2+}-dependent expression of Kv1.1 was more efficient in higher-CF neurons, proposing that neuronal tonotopic identity as well as pattern/level of afferent activity would be important for the tonotopic differentiation of Kv1.1 in NM (see Figure 6).

Activity-Dependence of Kv1.1 Expression Would Be Intrinsically Determined in a Tonotopic-Region-Specific Manner

In NM *in vivo*, Kv1 current increased efficiently with auditory input in higher-CF neurons, whereas the current remained small in low-CF neurons even after elevation of the input (Akter et al., 2018), leading to the idea that efficiency of neurons to drive Kv1.1 expression via auditory input would become higher toward the high-CF region in NM. The present study provided direct evidence to this idea. In the culture, Kv1 current

was down-regulated, comparable with that in immature animals (E15), and not different tonotopically even after maturation (14DIV). These would be attributed to the fact that the cultured NM neurons were deprived of both spontaneous and sound-driven inputs from the auditory nerve, which normally occur at high rates (100–500 Hz) and cause substantial depolarization *in vivo* (Fukui et al., 2006; Warchol and Dallos, 1990). Indeed, chronic depolarization increased Kv1 current particularly at high-CF regions and restored the tonotopic difference of the current in the culture. Thus, the activity-dependent mechanism of Kv1.1 expression would be programmed in a tonotopic-region-specific manner, which may underlie the tonotopic difference of the current in NM. These were consistent with the recent findings that couplings between neuronal activity and gene expression programs are determined differentially in individual neurons in the brain (Hrvatin et al., 2018; Kalish et al., 2018).

Importantly, the input-dependent increase of Kv1 current was small and either suppression or elevation of auditory input had only minor effects on the current during embryonic period *in vivo* (Akter et al., 2018). This contrasted with the observations that the depolarization increased Kv1 current substantially in the high-CF neurons irrespective of days in culture. One possible explanation for this discrepancy is that auditory input was limited in embryos owing to attenuation of sound through the eggshell and embryonic fluid (Jones et al., 2006), whereas the neurons were depolarized efficiently with the high-K^+ treatment in the culture. The results might indicate that the high efficiency to express Kv1.1 via auditory input is already equipped in NM neurons during early periods of maturation. Nevertheless, whether the period specificity for the Kv1.1 expression exists or not would require further studies *in vivo*.

Downstream Mechanism of Ca^{2+} Would Be Differentiated Tonotopically

Patterns and/or levels of afferent activities differ tonotopically in the auditory system (Fukui et al., 2006; Johnson et al., 2011; Lippe, 1995), which is considered crucial for the differentiations of auditory circuits (Kandler et al., 2009). This suggests that $[Ca^{2+}]_i$ in postsynaptic neurons plays a pivotal role in the differentiations (Friauf and Lohmann, 1999). This was the case in the differentiation of Kv1 current in NM. In support, homeostatic increase of Kv1 current was suppressed via chronic inhibition of Cav channels in cultured medial nucleus of trapezoid body (MNTB) neurons (Tong et al., 2010) or of NMDA receptors in cultured hippocampal neurons (Lee et al., 2015). In NM neurons, Cav1 channels would be activated via depolarization during synaptic and/or spike activities and work as a source of Ca^{2+} entry for the differentiation. In addition, AMPA receptors could be another source of Ca^{2+} entry *in vivo*, as synaptic activity is robust *in vivo* and the receptors are highly permeable to Ca^{2+} in NM (Trussell, 1999). On the other hand, contributions of NMDA receptors would be small, because expression of the receptors declines before hatch in NM (Lu and Trussell, 2007; Tang and Carr, 2007), whereas a major increase of Kv1 current occurs after hatch (Akter et al., 2018). In cultured NM neurons, a change in basal Ca^{2+} level was sufficient to cause the differentiation of Kv1 current, suggesting that overall activity is important for the differentiation. However, NM neurons receive different patterns of afferent input among tonotopic regions *in vivo* (Fukui and Ohmori, 2004; Fukui et al., 2006), and a possibility remains that a difference in Ca^{2+} transient further contributes to the differentiation. This difference in Ca^{2+} dynamics may explain why Kv1 current in low-CF neurons remained small in the culture even after the treatment with 3K medium (0.8 nA, Figure 4), compared with that in posthatch animals (1.5 nA, Akter et al., 2018).

The striking finding in the present study was that depolarization increased $[Ca^{2+}]_i$ similarly irrespective of tonotopic regions, indicating that the downstream mechanism of Ca^{2+} would be differentiated tonotopically in NM. As $[Ca^{2+}]_i$ necessary for Kv1.1 expression was rather low of around 100–200 nM (Figure 5; see also Awatramani et al., 2005), the mechanism may have rather high sensitivity to Ca^{2+} in high-CF neurons. This idea was consistent with the fact that a prolonged elevation of $[Ca^{2+}]_i$ above 250 nM promoted cell death in NM (Zirpel et al., 1998). In low-CF neurons, on the other hand, the high-K^+ treatment showed only a small increase of Kv1 current, and the mechanism of Kv1.1 expression may have lower sensitivity to Ca^{2+}. Interestingly, the expression of Ca^{2+}-binding proteins, such as calretinin and parvalbumin, differs along the tonotopic axis in NM (Wang et al., 2017). These tonotopic variations of Ca^{2+}-related molecules could be attributable to the fact that rhombomeres from which NM neurons arise are different depending on tonotopic regions (Cramer et al., 2000).

Kv1.1 mRNA increases toward the high-CF region in posthatch NM (Fukui and Ohmori, 2004). In addition, membranous localization of Kv1.1 protein increases in the high-CF region *in vivo* (Akter et al., 2018) and *in vitro* (Figure 3). Thus, the tonotopic difference in the mechanism of Kv1.1 expression may arise via

transcriptional regulation and/or posttranscriptional modification of Ca^{2+}-dependent molecules. As membrane trafficking of Kv1.1 is negatively regulated by ER-retention domain at the external pore region of the channel (Vacher and Trimmer, 2012), the molecules may include those that modulate the domain; matrix metalloprotease 23 could be a candidate molecule, because it binds to the domain and contributes to ER retention of Kv1.1, while it is released from the ER membrane via a Ca^{2+}-dependent cleavage by an endoprotease, furin (Galea et al., 2014; Rangaraju et al., 2010; Salvas et al., 2005). Alternatively, the molecules could be protein kinase C and/or protein kinase A, which were reported to increase synthesis and translocation of Kv1.1 protein (Levin et al., 1995; Winklhofer et al., 2003).

Functional Implication

Afferent activity contributes to tonotopic differentiation of ion-channel expression in both birds and mammals (Kuba et al., 2010; Leao et al., 2006; Akter et al., 2018; von Hehn et al., 2004). This is indeed the case in Kv1.1; it increases Kv1 current at the high-CF region in NM of chickens (Akter et al., 2018) and at the low-CF region in MNTB of mice (Leao et al., 2006). This discrepancy in the tonotopic regions could be related to the difference in audible frequency between the animals; it is much higher in mice (2–100 kHz, Heffner and Heffner, 2007) than in chickens (0.2–4 kHz, Saunders et al., 1973). Interestingly, the frequency range, at which the activity-dependent increase of Kv1 current occurs, is similar between the animals and comparable with the frequency, where temporal information is particularly important for auditory function (~2 kHz, Rayleigh, 1907). This may emphasize the importance of Kv1.1 in temporal coding in the auditory system (Kopp-Scheinpflug et al., 2003).

In the present study, we showed that the efficiency of translating $[Ca^{2+}]_i$ into Kv1.1 expression was fine-tuned in a tonotopic-region-specific manner, and it was higher at the high-CF region. The high efficiency would be beneficial for the high-CF neurons to ensure sufficient Kv1.1 expression, because the auditory threshold is high for high-frequency sound and the level of afferent input may not be high in the neurons (Saunders et al., 1973), whereas the low efficiency would be important for the low-CF neurons to prevent excess increase of Kv1.1 with auditory input. Thus, the topographic differentiation of activity-dependent mechanisms could be a secure and flexible way to ensure the optimum level of Kv1.1 expression at each tonotopic region and to shape precise and reliable temporal coding across frequencies. Interestingly, development of Kv3 current progressed independently of depolarization and tonotopic regions, indicating that expression of Kv channels is regulated in a subtype-specific manner. This is reasonable because Kv3.1 promotes spike generation and would be important for embryonic neurons to promote firing during the low level of afferent input. Thus, the activity-dependent process of ion-channel expression would be strategically designed in a tonotopic-region-specific manner for each channel type, which would ensure the precise temporal coding of sound across frequencies in the brainstem auditory circuit.

Limitation of Study

We showed in NM that the efficiency of activity-dependent Kv1.1 expression was determined in a tonotopic-region-specific manner, contributing to differentiating the channel expression within the nucleus. However, the data were obtained in slice culture, which preserves structures other than neurons, and further experiments in dissociate culture would be necessary to strengthen the conclusion that tonotopic neuronal identity is indeed different within the nucleus.

METHODS

All methods can be found in the accompanying Transparent Methods supplemental file.

SUPPLEMENTAL INFORMATION

Supplemental Information can be found online at https://doi.org/10.1016/j.isci.2019.02.022.

ACKNOWLEDGMENTS

This work was supported by grants-in-aid from MEXT (15H04257 to H.K., 16K07345 to R.A., 16K08493 to R.Y.) and Innovative Areas "Dynamic regulation of Brain Function by Scrap & Build" (17H05742) to H.K.

AUTHOR CONTRIBUTIONS

R.A. and H.K. designed research. R.A. and R.Y. performed research and analyzed data. R.A., R.Y., and H.K. wrote the paper.

DECLARATION OF INTERESTS

The authors declare no competing interests.

Received: July 24, 2018
Revised: December 17, 2018
Accepted: February 22, 2019
Published: March 29, 2019

REFERENCES

Akter, N., Adachi, R., Kato, A., Fukaya, R., and Kuba, H. (2018). Auditory input shapes tonotopic differentiation of Kv1.1 expression in avian cochlear nucleus during late development. J. Neurosci. *38*, 2967–2980.

Awatramani, G.B., Price, G.D., and Trussell, L.O. (2005). Modulation of transmitter release by presynaptic resting potential and background calcium levels. Neuron *48*, 109–121.

Babot, Z., Cristòfol, R., and Suñol, C. (2005). Excitotoxic death induced by released glutamate in depolarized primary cultures of mouse cerebellar granule cells is dependent on $GABA_A$ receptors and niflumic acid-sensitive chloride channels. Eur. J. Neurosci. *21*, 103–112.

Cramer, K.S., Fraser, S.E., and Rubel, E.W. (2000). Embryonic origins of auditory brain-stem nuclei in the chick hindbrain. Dev. Biol. *224*, 138–151.

Friauf, E., and Lohmann, C. (1999). Development of auditory brainstem circuitry. Activity-dependent and activity-independent processes. Cell Tissue Res. *297*, 187–195.

Fukui, I., and Ohmori, H. (2004). Tonotopic gradients of membrane and synaptic properties for neurons of the chicken nucleus magnocellularis. J. Neurosci. *24*, 7514–7523.

Fukui, I., Sato, T., and Ohmori, H. (2006). Improvement of phase information at low sound frequency in nucleus magnocellularis of the chicken. J. Neurophysiol. *96*, 633–641.

Galea, C.A., Nguyen, H.M., George Chandy, K., Smith, B.J., and Norton, R.S. (2014). Domain structure and function of matrix metalloprotease 23 (MMP23): role in potassium channel trafficking. Cell. Mol. Life Sci. *71*, 1191–1210.

Heffner, H.E., and Heffner, R.S. (2007). Hearing ranges of laboratory animals. J. Am. Assoc. Lab. Anim. Sci. *46*, 20–22.

Hrvatin, S., Hochbaum, D.R., Nagy, M.A., Cicconet, M., Robertson, K., Cheadle, L., Zilionis, R., Ratner, A., Borges-Monroy, R., Klein, A.M., et al. (2018). Single-cell analysis of experience-dependent transcriptomic states in the mouse visual cortex. Nat. Neurosci. *21*, 120–129.

Hyson, R.L., Reyes, A.D., and Rubel, E.W. (1995). A depolarizing inhibitory response to GABA in brainstem auditory neurons of the chick. Brain Res. *677*, 117–126.

Jhaveri, S., and Morest, D.K. (1982). Sequential alterations of neuronal architecture in nucleus magnocellularis of the developing chicken: a Golgi study. Neuroscience *7*, 837–853.

Johnson, S.L., Eckrich, T., Kuhn, S., Zampini, V., Franz, C., Ranatunga, K.M., Roberts, T.P., Masetto, S., Knipper, M., Kros, C.J., and Marcotti, W. (2011). Position-dependent patterning of spontaneous action potentials in immature cochlear inner hair cells. Nat. Neurosci. *14*, 711–717.

Johnston, J., Forsythe, I.D., and Kopp-Scheinpflug, C. (2010). Going native: voltage-gated potassium channels controlling neuronal excitability. J. Physiol. *588*, 3187–3200.

Jones, T.A., Jones, S.M., and Paggett, K.C. (2006). Emergence of hearing in the chicken embryo. J. Neurophysiol. *96*, 128–141.

Kalish, B.T., Cheadle, L., Hrvatin, S., Nagy, M.A., Rivera, S., Crow, M., Gillis, J., Kirchner, R., and Greenberg, M.E. (2018). Single-cell transcriptomics of the developing lateral geniculate nucleus reveals insights into circuit assembly and refinement. Proc. Natl. Acad. Sci. U S A *115*, E1051–E1060.

Kandler, K., Clause, A., and Noh, J. (2009). Tonotopic reorganization of developing auditory brainstem circuits. Nat. Neurosci. *12*, 711–717.

Köppl, C. (1994). Auditory nerve terminals in the cochlear nucleus magnocellularis: differences between low and high frequencies. J. Comp. Neurol. *339*, 438–446.

Kopp-Scheinpflug, C., Fuchs, K., Lippe, W.R., Tempel, B.L., and Rübsamen, R. (2003). Decreased temporal precision of auditory signaling in Kcna1-null mice: an electrophysiological study in vivo. J. Neurosci. *23*, 9199–9207.

Koyano, K., Funabiki, K., and Ohmori, H. (1996). Voltage-gated ionic currents and their roles in timing coding in auditory neurons of the nucleus magnocellularis of the chick. Neurosci. Res. *26*, 29–45.

Kuba, H., and Ohmori, H. (2009). Roles of axonal sodium channels in precise auditory time coding at nucleus magnocellularis of the chick. J. Physiol. *587*, 87–100.

Kuba, H., Oichi, Y., and Ohmori, H. (2010). Presynaptic activity regulates Na^+ channel distribution at the axon initial segment. Nature *465*, 1075–1078.

Kuba, H., Yamada, R., Ishiguro, G., and Adachi, R. (2015). Redistribution of Kv1 and Kv7 enhances neuronal excitability during structural axon initial segment plasticity. Nat. Commun. *6*, 8815.

Leao, R.N., Sun, H., Svahn, K., Berntson, A., Youssoufian, M., Paolini, A.G., Fyffe, R.E., and Walmsley, B. (2006). Topographic organization in the auditory brainstem of juvenile mice is disrupted in congenital deafness. J. Physiol. *571*, 563–578.

Lee, K.Y., Royston, S.E., Vest, M.O., Ley, D.J., Lee, S., Bolton, E.C., and Chung, H.J. (2015). N-methyl-D-aspartate receptors mediate activity-dependent down-regulation of potassium channel genes during the expression of homeostatic intrinsic plasticity. Mol. Brain *8*, 4.

Levin, G., Keren, T., Peretz, T., Chikvashvili, D., Thornhill, W.B., and Lotan, I. (1995). Regulation of RCK1 currents with a cAMP analog via enhanced protein synthesis and direct channel phosphorylation. J. Biol. Chem. *270*, 14611–14618.

Lippe, W.R. (1995). Relationship between frequency of spontaneous bursting and tonotopic position in the developing avian auditory system. Brain Res. *703*, 205–213.

Lu, Y., and Rubel, E.W. (2005). Activation of metabotropic glutamate receptors inhibits high-voltage-gated calcium channel currents of chicken nucleus magnocellularis neurons. J. Neurophysiol. *93*, 1418–1428.

Lu, T., and Trussell, L.O. (2001). Mixed excitatory and inhibitory GABA-mediated transmission in chick cochlear nucleus. J. Physiol. *535*, 125–131.

Lu, T., and Trussell, L.O. (2007). Development and elimination of endbulb synapses in the chick cochlear nucleus. J. Neurosci. *27*, 808–817.

Monsivais, P., Yang, L., and Rubel, E.W. (2000). GABAergic inhibition in nucleus magnocellularis: implications for phase locking in the avian auditory brainstem. J. Neurosci. *20*, 2954–2963.

Oertel, D. (1999). The role of timing in the brain stem auditory nuclei of vertebrates. Annu. Rev. Physiol. *61*, 497–519.

Oline, S.N., Ashida, G., and Burger, R.M. (2016). Tonotopic optimization for temporal processing in the cochlear nucleus. J. Neurosci. *36*, 8500–8515.

Parameshwaran, S., Carr, C.E., and Perney, T.M. (2001). Expression of the Kv3.1 potassium channel in the avian auditory brainstem. J. Neurosci. *21*, 485–494.

Parks, T.N., and Rubel, E.W. (1978). Organization and development of the brain stem auditory nuclei of the chicken: primary afferent projections. J. Comp. Neurol. *180*, 439–448.

Rangaraju, S., Khoo, K.K., Feng, Z.-P., Crossley, G., Nugent, D., Khaytin, I., Chi, V., Pham, C., Calabresi, P., Pennington, M.W., et al. (2010). Potassium channel modulation by a toxin domain

in matrix metalloprotease 23. J. Biol. Chem. *285*, 9124–9136.

Rathouz, M., and Trussell, L. (1998). Characterization of outward currents in neurons of the avian nucleus magnocellularis. J. Neurophysiol. *80*, 2824–2835.

Rayleigh, L. (1907). On our perception of sound direction. Philos. Mag. *13*, 214–232.

Reyes, A.D., Rubel, E.W., and Spain, W.J. (1994). Membrane properties underlying the firing of neurons in the avian cochlear nucleus. J. Neurosci. *14*, 5352–5364.

Salvas, A., Benjannet, S., Reudelhuber, T.L., Chrétien, M., and Seidah, N.G. (2005). Evidence for proprotein convertase activity in the endoplasmic reticulum/early Golgi. FEBS Lett. *579*, 5621–5625.

Sanchez, J.T., Seidl, A.H., Rubel, E.W., and Barria, A. (2011). Preparation and culture of chicken auditory brainstem slices. J. Vis. Exp. *49*, https://doi.org/10.3791/2527.

Saunders, J.C., Coles, R.B., and Gates, G.R. (1973). The development of auditory evoked responses in the cochlea and cochlear nuclei of the chick. Brain Res. *63*, 59–74.

Sullivan, W.E., and Konishi, M. (1984). Segregation of stimulus phase and intensity coding in the cochlear nucleus of the barn owl. J. Neurosci. *4*, 1787–1799.

Tang, Y.Z., and Carr, C.E. (2007). Development of N-methyl-D-aspartate receptor subunits in avian auditory brainstem. J. Comp. Neurol. *502*, 400–413.

Tong, H., Steinert, J.R., Robinson, S.W., Chernova, T., Read, D.J., Oliver, D.L., and Forsythe, I.D. (2010). Regulation of Kv channel expression and neuronal excitability in rat medial nucleus of the trapezoid body maintained in organotypic culture. J. Physiol. *588*, 1451–1468.

Trussell, L.O. (1999). Synaptic mechanisms for coding timing in auditory neurons. Annu. Rev. Physiol. *61*, 477–496.

Vacher, H., and Trimmer, J.S. (2012). Trafficking mechanisms underlying neuronal voltage-gated ion channel localization at the axon initial segment. Epilepsia *53*, 21–31.

von Hehn, C.A., Bhattacharjee, A., and Kaczmarek, L.K. (2004). Loss of Kv3.1 tonotopicity and alterations in cAMP response element-binding protein signaling in central auditory neurons of hearing impaired mice. J. Neurosci. *24*, 1936–1940.

Wang, X., Hong, H., Brown, D.H., Sanchez, J.T., and Wang, Y. (2017). Distinct neural properties in the low-frequency region of the chicken cochlear nucleus magnocellularis. eNeuro *4*, e0016–17.

Warchol, M.E., and Dallos, P. (1990). Neural coding in the chick cochlear nucleus. J. Comp. Physiol. *166*, 721–734.

Winklhofer, M., Matthias, K., Seifert, G., stocker, M., Sewing, S., Herget, T., Steinhäuser, C., and Saaler-Reinhardt, S. (2003). Analysis of phosphorylation-dependent modulation of Kv1.1 potassium channels. Neuropharmacology *44*, 829–842.

Zirpel, L., Lippe, W.R., and Rubel, E.W. (1998). Activity-dependent regulation of $[Ca^{2+}]i$ in avian cochlear nucleus neurons: roles of protein kinases A and C and relation to cell death. J. Neurophysiol. *79*, 2288–2302.

ISCI, Volume *13*

Supplemental Information

Tonotopic Differentiation of Coupling between Ca^{2+} and Kv1.1 Expression in Brainstem Auditory Circuit

Ryota Adachi, Rei Yamada, and Hiroshi Kuba

Supplemental Figures

Figure S1

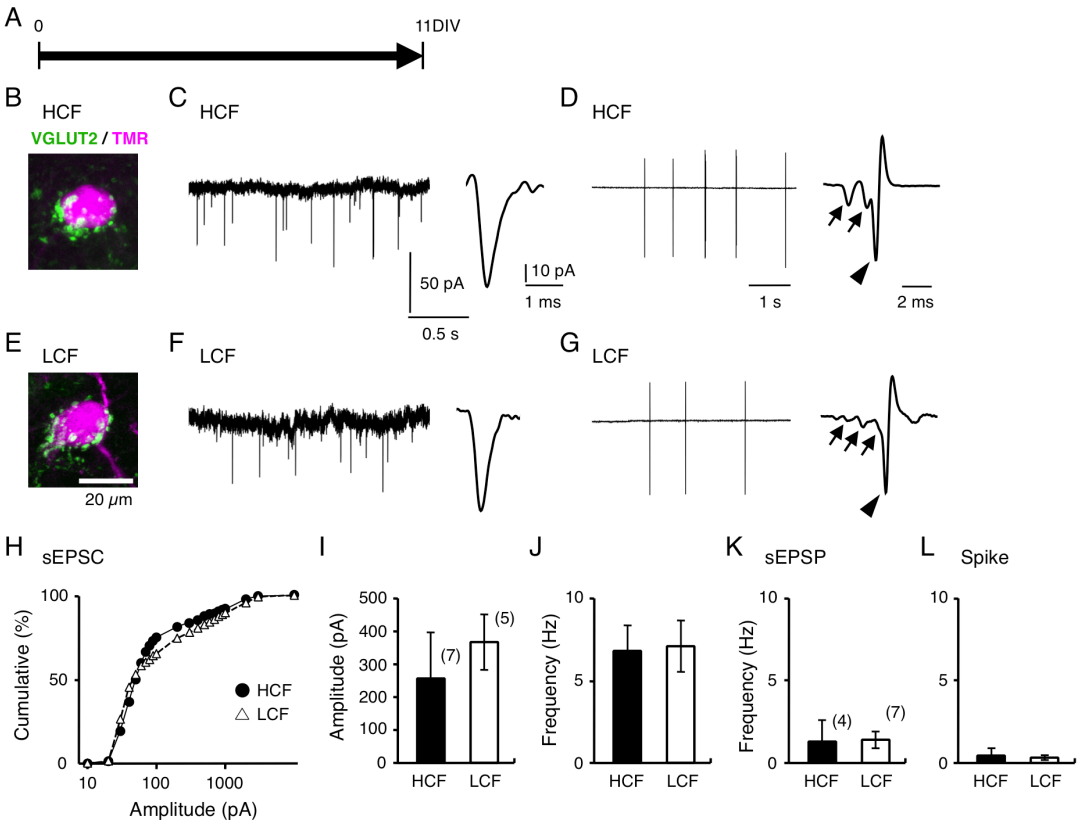

Figure S1. Spontaneous activities in slice culture. Related to Figure 1.

(A) Synaptic terminals and activities were evaluated at 11DIV. (B and E) VGLUT2-positive terminals (green) surrounded TMR-labeled neurons (magenta) at high- (B) and low-CF (E) regions. These terminals were presumably from surrounding neurons, as projections from contralateral NM were distributed more ventrally (Figure 1C lower right, arrowhead). (C and F) Spontaneous EPSCs in high- (C) and low-CF (F) neurons. Expanded traces (inset). (D and G) Spontaneous activities recorded under cell-attached clamp in high- (D) and low-CF (G) neurons. Expanded traces (inset). Spontaneous EPSPs were identified as small negative responses (arrows), some of which accompanied large biphasic spike responses (arrowhead). These responses were occluded by DNQX (20 μM). (H–J) Cumulative amplitude plot (H), amplitude (I), and frequency (J) of spontaneous EPSCs. (K and L) Frequency of spontaneous EPSPs (K) and spikes (L). Note that frequency of sEPSPs was far lower than that of sEPSCs, presumably because cell-attached recording could not detect small quantal events.

Figure S2

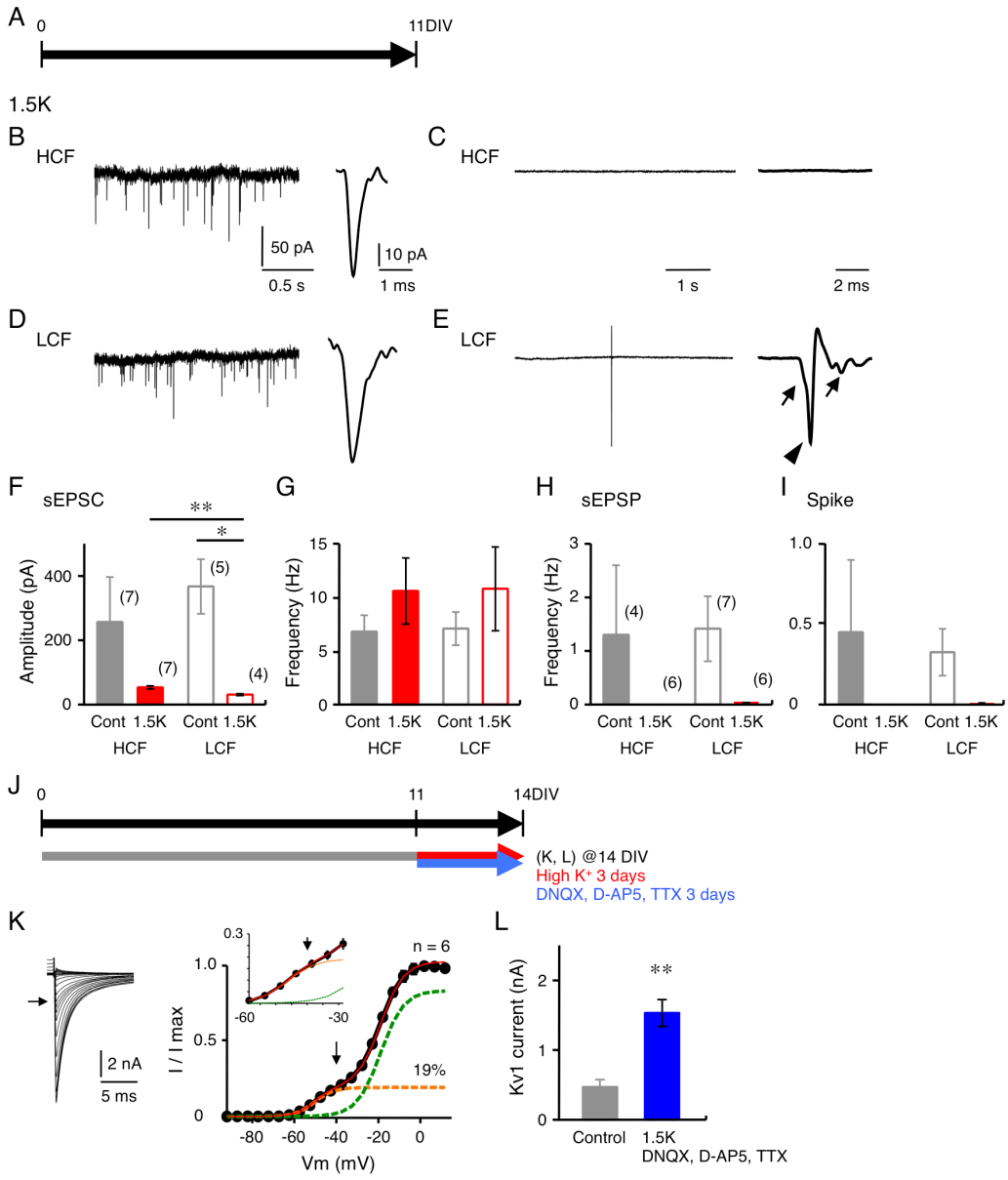

Figure S2. Increase of Kv1 current occurred without synaptic and spike activities. Related to Figures 2, 4, and S1.

(A) Neurons were cultured in normal medium and recordings were made at 11DIV in 1.5K medium. (B and D) Spontaneous EPSCs in high- (B) and low-CF (D) neurons. Expanded traces (inset). (C and E) Spontaneous EPSPs and spikes recorded under cell-attached clamp in high- (C) and low-CF (E) neurons. Expanded traces (inset). (F and G) Amplitude (F) and frequency (G) of spontaneous EPSCs. Controls were from

Figure S1I and S1J (grey). (H and I) Frequency of spontaneous EPSPs (H) and spikes (I). Controls were from Figure S1K and S1L (grey). (J–L) Effects of synaptic and spike activities on Kv1 current during chronic 1.5K treatment in high-CF neurons. Slices were cultured in 1.5K medium in the presence of TTX (0.1 μM), DNQX (20 μM) and D-AP5 (100 μM) for 11-14DIV (J). Tail current (left) and conductance-voltage curve (right) (K). Magnified curve (inset). Kv1 current calculated at +20 mV (L). Control was from Figure 2J (grey). Note that Kv1 current increased even under blockade of synaptic activities, suggesting that postsynaptic depolarization would be sufficient to induce the increase of Kv1 current. * $p < 0.05$, ** $p < 0.01$.

Figure S3

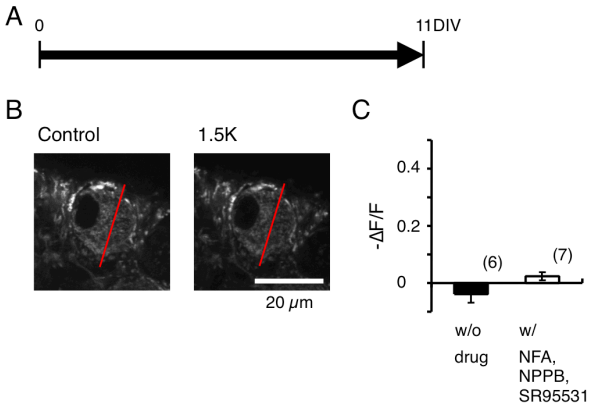

Figure S3. Intracellular Cl^- level would not change during high-K^+ treatment. Related to Figure 4.

Two-photon Cl^- imaging in high-CF neurons. Cells were loaded with a Cl^- indicator (MQAE) at 11DIV after cultured in normal medium (A). Images captured before (left) and 5–20 min after (right) perfusion of 1.5K medium (B). Red lines indicate location of line scans. Change of Cl^- signal ($-\Delta F/F$) during 1.5K treatment (C). Cl^- signal was not altered during 1.5K treatment with or without a cocktail of Cl^- channel blockers (10 μM SR95531, 100 μM niflumic acid, and 200 μM NPPB), suggesting that elevation of $[K^+]_o$ would have little effects on intracellular Cl^- level in the neurons.

Figure S4

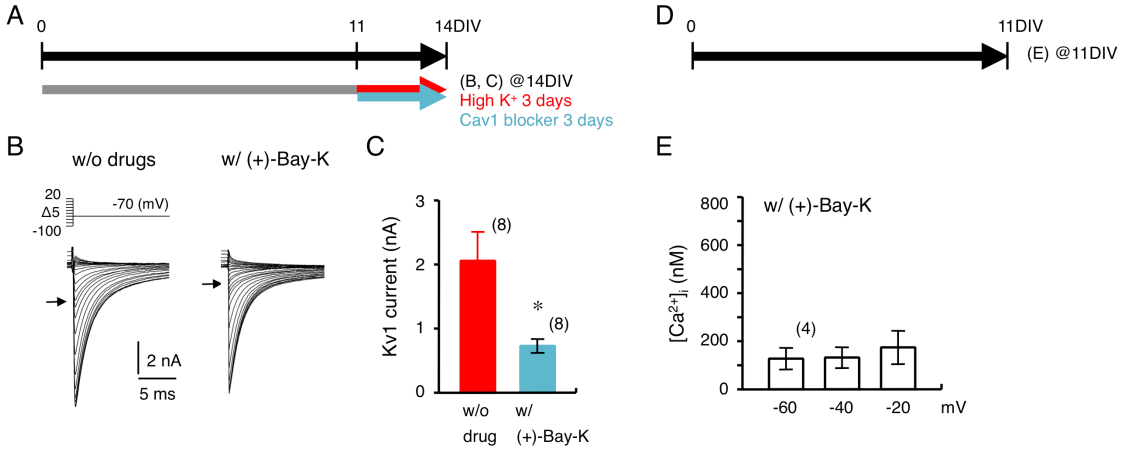

Figure S4. Ca^{2+} entry through Cav1 channels would be crucial for the increase of Kv1 current during high-K^+ treatment. Related to Figure 5.

(A) $[K^+]_o$ in culture medium was elevated by 1.5 times, while (+)-Bay-K8644 (5 μM, blocker of Cav1) was applied for 11–14DIV in high-CF neurons. (B) Tail current without (left) and with (+)-Bay-K8644 (right). Arrows indicate tail current at –40 mV, and roughly represents Kv1 current. (C) Kv1 current calculated at +20 mV. Data in 1.5K treatment (red) were from Figure 4G. (D) Neurons were cultured in normal medium and imaging was made at 11DIV. (E) Dependence of $[Ca^{2+}]_i$ on membrane depolarization with (+)-Bay-K8644. Numbers in parentheses are the number of cells. * $p < 0.05$.

Figure S5

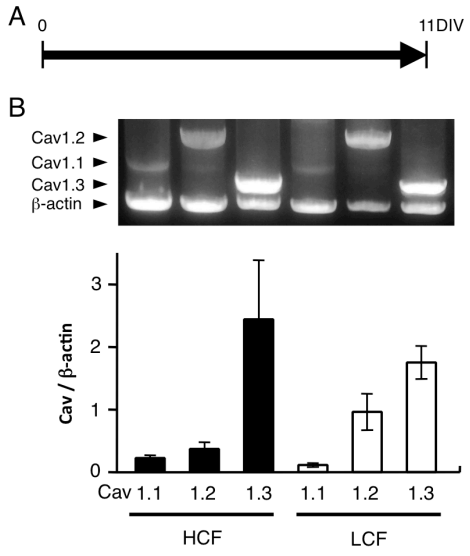

Figure S5. Cav1 mRNAs were expressed at high- and low-CF regions. Related to Figure 5.

(A) Slices were cultured in normal culture medium and mRNA was extracted at 11DIV.

(B) Cav1 and β-actin gene expression at high- and low-CF regions. Among four types of Cav1 channels, Cav1.1, Cav1.2, and Cav1.3 were identified in chickens. mRNA levels of three types of Cav1 channels and β-actin were analyzed by RT-PCR (upper). Level of Cav1 mRNAs relative to that of β-actin was not different between high- and low-CF regions for each subtype (lower).

Figure S6

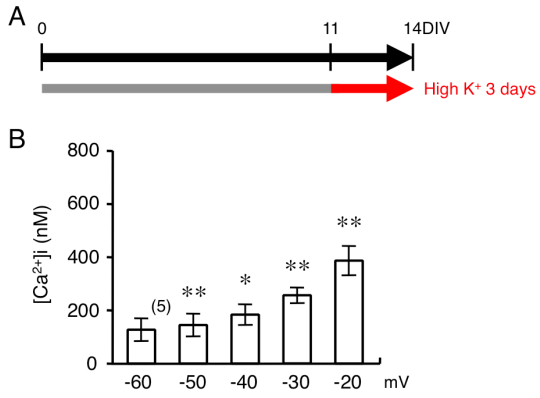

Figure S6. Voltage dependence of Ca^{2+} level at the end of high-K^+ treatment. Related to Figure 5.

Two-photon Ca^{2+} imaging in 1.5K medium after 3-day incubation in the medium. (A) High-CF neurons were loaded with Fluo-5F through a patch pipette at 14DIV, and $[Ca^{2+}]_i$ was measured under voltage clamp. (B) Dependence of $[Ca^{2+}]_i$ on membrane depolarization. Note that $[Ca^{2+}]_i$ was still dependent on depolarization at the end of high-K^+ treatment, and the level of $[Ca^{2+}]_i$ was similar to that measured at 11DIV in normal ACSF ($p > 0.1$ at each potential, see Fig. 5I). * $p < 0.05$, ** $p < 0.01$ compared with –60 mV.

Transparent Methods

Animals. Chickens (*Gallus domesticus*) of E11 were used for organotypic slice culture. All animal procedures in this study were approved by the Nagoya University Animal Experiment Committee.

Preparation of organotypic slice culture. Chick embryos were anesthetized by cooling eggs in ice-cold water. The brainstem was removed and dissected in a high-glucose artificial cerebrospinal fluid (HG-ACSF) (concentration in mM; 75 NaCl, 2.5 KCl, 26 $NaHCO_3$, 1.25 NaH_2PO_4, 1 $CaCl_2$, 3 $MgCl_2$ and 100 glucose, pH7.3) bubbled with 95% O_2 and 5% CO_2. Retrograde labeling of NM neurons and anterograde labeling of their terminals were made by injecting dextran (MW 3000) conjugated with TMR (Life Technologies, 10–40% in 0.1 M phosphate buffer adjusted to pH 2.0 with HCl) into the midline tract region through a patch pipette and incubating the brainstem in the HG-ACSF for 30 min at 38 ˚C (Lawrence and Trussell, 2000; Wirth et al., 2008). Four to five coronal slices (200 μm) were obtained with a vibratome (VT1200, Leica) (Figure 1B). Slices containing high- or low-CF region of NM (Figure 1 legends) were collected, transferred on a Millicell membrane insert (Millipore) in a culture dish (35 mm), and cultured until 14DIV in Neurobasal medium (Life Technologies) containing 2% B-27 serum-free supplement (Life Technologies), 1 mM glutamate solution (Life Technologies), and 1% penicillin-streptomycin solution (Wako). During the first 4 days, 5% fetal bovine serum (Biowest) was added, and half of the medium was changed twice a week. NM neurons were depolarized for either 3 or 13 days by adding KCl to the medium (Figures 3–5). Cav channels were blocked with 10 μM nifedipine (Sigma), (+)-Bay-K8644 (5 μM, Cayman), 2 μM ω-conotoxin GVIA (Peptide Institute), 0.2 μM ω-agatoxin IVA (Peptide Institute), 0.1 mM $NiCl_2$, and/or 2 μM TTA-P2 (Merck) for 3 days between 11DIV and 14DIV (Figures 5 and S4). Voltage-gated Na^+ channels were blocked with 0.1 μM TTX (Wako), and excitatory synaptic responses were blocked with 20 μM DNQX (Sigma) and 100 μM D-AP5 (Alomone) for 3 days between 11DIV and 14DIV (Figure S2).

Immunohistochemistry. NM neurons were labeled by injecting dextran TMR into the midline of cultured slices 2 hrs before fixation. Slices were fixed with a periodate-lysine-paraformaldehyde fixative (1% paraformaldehyde, 2.7% lysine HCl,

0.21% $NaIO_4$, and 2.85 mM Na_2HPO_4) for 30 min at 4˚C. Non-specific binding of antibodies was reduced by incubating the slices for 1 hr with PBS containing 1% donkey serum, 0.05% carrageenan, and 0.1% Triton X-100. The primary antibodies used were as follows; mouse monoclonal VGLUT2 antibody (5 µg/ml, clone N29/29, NeuroMab), rabbit polyclonal Kv1.1 antibody (1.8 µg/ml, Alomone), and rabbit polyclonal TRITC (TMR) antibody (2.5 µg/ml, Life Technologies). After overnight incubation with the primary antibodies at room temperature, slices were incubated with secondary antibodies conjugated with Alexa (Life Technologies) for 2 hrs, mounted on a slide glass, cover-slipped, and observed under a confocal laser-scanning microscope (FV1000, Olympus) with a ×40, 0.9-NA objective (Olympus). For quantification of Kv1.1 signal, images were captured with the same microscope setting without z-stack. Signal intensity was measured along a line across a cell including the maximum membranous signals but excluding the nucleus, and relative intensity between membranous and cytoplasmic signals was calculated from three lines in each cell. Membranous signal was defined as the signal within 1–2 µm from the edge, and cytoplasmic signal as that between the membranous signals. The edge was defined as the point at which signals fell below 80% of cytoplasmic signal. Background signal was not subtracted.

Electrophysiology. Whole-cell and cell-attached patch-clamp recordings were made with Multiclmap 700B (Molecular Device), as described (Akter et al., 2018). Recording temperature was 37–38˚C, unless otherwise stated. For current-clamp recording, slices were perfused with ACSF (in mM: 125 NaCl, 2.5 KCl, 26 $NaHCO_3$, 1.25 NaH_2PO_4, 2 $CaCl_2$, 1 $MgCl_2$, 17 glucose, pH 7.3). Pipettes were pulled from glass capillary (Harvard Apparatus) with a puller (Sutter Instruments) and had a resistance of 3–4 MΩ when filled with a K^+-based internal solution (in mM: 113 K-gluconate, 14 $Tris_2$-phosphocreatine, 4.5 $MgCl_2$, 4 Na_2-ATP, 0.3 Tris-GTP, 0.2 EGTA, and 9 HEPES-KOH, pH 7.2). Whole-cell and cell-attached recordings of spontaneous synaptic and spike currents were made in the culture media, while a pipette was filled with the K^+-based internal solution. Concentration of $CaCl_2$ in the culture media was 1.8 mM. For whole-cell recording of K^+ current, a pipette was filled with a Cs^+-based internal solution (in mM: 155 $CsMeSO_3$, 5 NaCl, 1.5 $MgCl_2$, 0.2 EGTA, 10 HEPES-CsOH, pH7.2), while $[K^+]_o$ was increased to 5 mM, $[Ca^{2+}]_o$ was decreased to

0.5 mM, and $CdCl_2$ (1 mM), $NiCl_2$ (0.5 mM), TTX (1 μM), SR95531 (10 μM, Abcam) and DNQX (20 μM) were added to the bath. Recordings were made at 20 ˚C to improve voltage clamp (Kuba et al., 2015). Reversal potential of the current was –26 mV, similar to the theoretical value with a permeability ratio of 0.1 between Cs^+ and K^+ (Kuba et al., 2015; Rathouz and Trussell, 1998). Series resistance was compensated electronically up to 80%. Liquid junction potentials were 11.6 mV for current clamp and 6.9 mV for whole-cell voltage clamp, and corrected after experiments. Voltage and current responses were analyzed, as described (Akter et al., 2018). For recording of spikes, current pulses were applied at an interval of 1-2 sec with an increment of 50 pA. Threshold current was defined as the minimum current required for spike generation, and spike parameters were measured at 0.1 nA above the threshold current, as reported previously (Akter et al., 2018). Membrane parameters were measured via injection of a current (50 pA) under current clamp. Input resistance (R_m) was measured at pulse end, membrane time constant (τ_m) by fitting to an exponential function, and membrane capacitance (C_m) from the R_m and τ_m. Depolarizing effect of high-K^+ treatment was evaluated at the beginning (11DIV) and the end (14DIV) of the treatment by measuring membrane potential in the media. Conductance-voltage curve of Kv current was fitted to a double Boltzmann equation; $I/I\mathrm{max} = A1/\{1 + \exp[-(V_m - V_{1/2}1)/S1]\} + A2/\{1 + \exp[-(V_m - V_{1/2}2)/S2]\}$, where I is the tail current amplitude, Imax is the maximum tail current amplitude, V_m is the membrane potential, $A1$ and $A2$ are weighting factors, $V_{1/2}1$ and $V_{1/2}2$ are half-activation voltages, and $S1$ and $S2$ are slope factors of individual components (Kuba et al., 2015; Rathouz and Trussell, 1998). Amplitude of Kv1 current was defined as a fraction of Kv1 component in the maximum tail current measured at +20 mV. Effects of high-K^+ treatment on Kv currents were evaluated either unblind or blind, and the results were similar in both cases; Kv1 current was 2.4±0.3 nA (n = 11) and 3.4±0.5 nA (n = 3) for unblind and blind, respectively, in 1.5K medium in high-CF neurons (p = 0.35).

Two-photon Ca^{2+} imaging. Two-photon Ca^{2+} imaging was performed as described in Fukaya et al. (2018). A Ti:sapphire pulsed laser (MaiTai DeepSee-OL, Spectra Physics) powered a FV1000MPE two-photon imaging system (Olympus). The laser was tuned to 810 nm. The K^+-based internal solution included a high-affinity dye (Oregon Green 488 BAPTA-1, OGB-1, 200 μM, Life Technologies, green) or a low-affinity dye (Fluo-5F,

250 μM, Life Technologies, green), and a volume marker (Alexa 594, 10 μM, Life Technologies, red), while EGTA was omitted. ACSF was circulated, unless otherwise stated, and TTX (1 μM), DNQX (20 μM), D-AP5 (100 μM) and SR95531 (10 μM) were added to the bath. Recordings were made at 30˚C. Fluorescence signal was captured through a ×25, 1.05-NA objective (Olympus). Fluorescence was split into green and red channels using a dichroic mirror (SDM570) and bandpass filters (FF01-510/84-25 and FF01-630/92-25), and then focused on a GaAsP detector for green and a photomultiplier tube for red. Data were collected at the soma in the line-scan mode at 4–5 ms/line (20 μs/pixel), including mirror flyback. Data are presented as averages of 10–20 events per site, and expressed as $\Delta(G/R)/(G/R)_0*100$ for OGB-1, and $[(G/R)–(G/R)_{min}]/[(G/R)_{max}–(G/R)]*K_D$ for Fluo-5F, where $(G/R)_0$ is the fluorescence at –70 mV, $(G/R)_{min}$ and $(G/R)_{max}$ are the minimal fluorescence at 2 mM EGTA and maximal fluorescence at 2 mM Ca^{2+}, respectively, and K_D is dissociation constant of Fluo-5F (1.3 μM at 34 ˚C) (Yasuda et al., 2004). Ca^{2+} level at each potential was calculated as an average of 1.3–1.5 s.

Two-photon Cl^- imaging. Two-photon Cl^- imaging was performed with a Cl^- dye (MQAE, n-6-methoxyquinolyl acetoethyl ester, Biotium) (Marandi et al., 2002). A slice was incubated in culture medium containing 6 mM MQAE for 10 min at 37 ˚C, and then washed in dye-free medium for 10 min at room temperature. During imaging, the slice was perfused with the normal culture medium, and then with high-K^+ medium (1.5K). The temperature was 30 ˚C. The laser was tuned to 810 nm, and fluorescence signal peaked at 460 nm was captured with the filter setting described above. Line scans were made at the soma for 100 ms in each cell (4–5 ms/line, 20 μs/pixel), and signal for a cell was calculated as an average of the period. Data are expressed as $–\Delta F/F_0*100$, where F_0 is the baseline fluorescence in the normal medium. Contributions of Cl^- channels to $[Cl^-]_i$ were evaluated by blocking the channels with SR95531 (10 μM), niflumic acid (100 μM, R&D systems), and NPPB (200 μM, R&D systems).

Semiquantitative RT-PCR. Total RNA was extracted from tissues in high- and low-CF region of NM using the Nucleospin RNA kit (Takara). cDNA synthesis and PCR were performed using the ReverTra Ace qPCR RT kit (Toyobo) and the KOD FX Neo (Toyobo), respectively. Primers using in this study are as follows; Cav1.1 forward,

TCCATCAATGGCACTGAGTG; Cav1.1 reverse, ACAGCCTTCTCTTTCAGCTG; Cav1.2 forward, ACTTCTCTTTCACCCCAACG; Cav1.2 reverse, TTCCTAAAGGAGAGGTGTCG; Cav1.3 forward, ACAGCGCAAGAATCTCCATC; Cav1.3 reverse, TGAATCTCGTCTGTCACTGC; β-actin forward, ATGATGATATTGCTGCGCTC; β-actin reverse, CATGATGGAGTTGAAGGTAG. PCR products were separated by 1.2% agarose gel. The intensity of band was measured using ImageJ software, and Cav signal was normalized by that of β-actin.

Statistics. Normality of data and equality of variance were evaluated by Shapiro-Wilk test and F-test, respectively. Statistical significance was determined with two-tailed Student's *t*-test or Wilcoxon rank sum test for comparison between two groups, and with ANOVA and *post hoc* Tukey test for comparison among more than three groups. In the result of Ca^{2+} imaging (Figures 5, S4 and S6), paired two-tailed *t*-test was used. Values are presented as the mean ± SE.

Supplemental References

Fukaya, R., Yamada, R., and Kuba, H. (2018). Tonotopic variation of the T-type Ca^{2+} current in avian auditory coincidence detector neurons. J. Neurosci. *38*, 335–346.

Lawrence, J.J., and Trussell, L.O. (2000). Long-term specification of AMPA receptor properties after synapse formation. J. Neurosci. *20*, 4864–4870.

Marandi, N., Konnerth, A., and Garaschuk, O. (2002). Two-photon chloride imaging in neurons of brain slices. Pflugers Arch. *445*, 357–365.

Wirth, M.J., Kuenzel, T., Luksch, H., and Wagner, H. (2008). Identification of auditory neurons by retrograde labelling for patch-clamp recording in a mixed culture of chick brainstem. J. Neurosci. Methods *169*, 55–64.

Yasuda, R., Nimchinsky, E.A., Scheuss, V., Pologruto, T.A., Oertner, T.G., Sabatini, B.L., and Svoboda, K. (2004). Imaging calcium concentration dynamics in small neuronal compartments. Sci. STKE *219*, pl5.